THESIS

THE CONFORMAL PERFECTLY MATCHED LAYER FOR ELECTRICALLY LARGE CURVILINEAR HIGHER ORDER FINITE ELEMENT METHODS IN ELECTROMAGNETICS

Submitted by

Aaron P. Smull

Department of Electrical and Computer Engineering

In partial fulfillment of the requirements

For the Degree of Master of Science

Colorado State University

Fort Collins, Colorado

Summer 2017

Master's Committee:

Advisor: Branislav Notaros

Ali Pezeshki
Donald Estep

ABSTRACT

THE CONFORMAL PERFECTLY MATCHED LAYER FOR ELECTRICALLY LARGE CURVILINEAR HIGHER ORDER FINITE ELEMENT METHODS IN ELECTROMAGNETICS

The implementation of open-region boundary conditions in computational electromagnetics for higher order finite element methods presents a well known set of challenges. One such boundary condition is known as the perfectly matched layer. In this thesis, the generation of perfectly matched layers for arbitrary convex geometric hexahedral meshes is discussed, using a method that can be implemented without differential operator based absorbing boundary conditions or coupling to boundary integral equations.

A method for automated perfectly matched layer element generation is presented, with geometries based on surface projections from a convex mesh. Material parameters are generated via concepts from transformation electromagnetics, from complex-coordinate transformation based conformal PML's in existing literature. A material parameter correction algorithm is also presented, based on a modified gradient descent optimization algorithm

Numerical results are presented with comparison to analytical results and commercial software, with studies on the effects of discretization error of the effectiveness of the perfectly matched layer. Good agreement is found between simulated and analytical results, and between simulated results and commercial software.

ACKNOWLEDGEMENTS

I am grateful most of all to my family, whose support and love through the years has brought me continued fortune in my education. I would like to thank my advisor, Dr. Branislav Notaros, whose support and guidance proved, and without whom I would have never entered into academic research. Additionally, I would like to thank my committee members for their invaluable input, as well as the entire staff and faculty for their assistance in my academic and professional development. Finally, I would like to acknowledge the current and past, Ana, Sanja, Elene, Nada, Cameron, Pranav, and Nabeel, each of whom put up with my constant questionings, proved very useful as a resource for discussion, and kept me entertained throughout my countless hours in the lab.

TABLE OF CONTENTS

LIST OF FIGURES

CHAPTER 1: INTRODUCTION

1.1 Computational Electromagnetics

The most important and influential development in engineering electromagnetics during the late 20th century was the advent of numerical methods to quickly and efficiently discretize and solve the complicated boundary value problem resulting from the Maxwell's equations. Since, such boundary value problems are rarely solvable by analytical methods except for in the most simple of geometries [1], the exact computation of fields in electromagnetic devices was nearly impossible prior to the development of modern computational tools.

Modern computational methods in electromagnetics are roughly divided into two categories. The first of these is the branch of asymptotic numerical methods. As has been known and studied for years, in a high-frequency limit, the propagation of electromagnetic field can be understood almost entirely in geometric terms, through the use of ray approximations and geometrical optics [2]. The physical optics (PO) (physical optics) method [3] represents a midway point between the absolute geometrical regime and the full-wave regime, in which . Alternatively, at long ranges or low frequencies, the fast multipole method (FMM) [4] can be used as an approximative method. At large separations, the interaction between two electromagnetic sources can be well approximated in terms of low-order spherical multipole expansions [5], from which fast numerical techniques can be used to quickly calculate an effective electromagnetic interaction. While the asymptotic methods discussed are often accurate to a first approximation in the case of electrically large, smooth, and homogeneous bodies, they lack the ability to fully model the myriad of diffraction and interference effects that may occur in the presence of highly varying geometries or material compositions. Most often, asymptotics

such as these do not serve the purpose of providing a fully accurate physical model, and thus cannot be used effectively in engineering design.

The second branch of numerical methods is that of full-wave methods. These are methods which explicitly discretize Maxwell's equations into sets of linear equations, which are solved over fully discretized physical domains. These include methods such as the class of finite difference methods (FD), which the approximate derivatives in a set of differential equations via algebraic difference equations, and the method of moments (MoM), which discretizes and solves a surface integral equation based on minimization of a residual over a chosen basis space. Often times, a type of full-wave analysis can be combined with one of the full, such as in the case of the multi-level fast multipole method used in the method of moments (MLFMM).

One full-wave numerical method in particular, the finite element method (FEM), was developed in the early 20th century and later popularized in the 1960's by NASA's NASTRAN program as a way to solve the boundary value problems arising from analyzing the structural dynamics of arbitrarily shaped elastic bodies [6]. The FEM has continued to show widespread use and development through the late 20th and early 21st centuries, in the fields of fluid dynamics [7], thermodynamic analysis [8], and a wide variety of other engineering disciplines. Somewhat more recently, finite elements worked their way into the electromagnetics [1] where they have remained one of the most powerful and versatile tools available.

1.2 Open-Domain Problems

Oftentimes physical problems in the computational sciences present natural boundary conditions and can be cast as boundary value problems in differential form, to which a variety of well-developed numerical techniques are available for analysis. While a subset of problems in

electromagnetics does give rise to natural boundary conditions, the topic of wave propagation modeling is somewhat unique in that, in a majority of cases, no natural boundaries exist. In fact, since the electromagnetic field is carried by the medium of the vacuum itself, there are hardly any limitations whatsoever on the extent of propagation. One of the prominent challenges of computational electromagnetics has been the implementation of open-domain problems. Absent of electric containment through conducting walls or faraday cages, electromagnetic fields generally propagate throughout all of space. Since volume discretization methods such as the finite-difference time-domain (FDTD) [9] method and the finite element method [1] require the explicit modeling of electromagnetic fields throughout the domain of interest, a problem is introduced when attempting to solve these problems – it is, of course, not possible to simulate an infinite domain of electric fields on a computer with finite memory or time. Any attempt to simply truncate the domain of interest leads to its own problems – setting the fields to zero at boundaries is equivalent to truncation of the domain in a perfectly electrically conducting box. As is well known, this type of truncation leads to reflected waves, which are generally not representative of the physics involved in a true open-domain simulation (referred to in literature as spurious modes).

It is of interest in electromagnetics to examine the behavior of an electronic devices in environments isolated from interaction with external interference. For example, when designing and testing an antenna, measurements of values such as the input reflection coefficient, $S_{11,}$ are typically made in an open-domain simulating anechoic chamber [10]. These chambers consist of electrically isolated rooms filled on the inside with radio-frequency (RF) absorbers. Typically, the types of absorbers used are pyramids made of lossy material, sized so as to ensure the gaps between adjacent pyramid tips do not exceed 1λ.

The physical problem can be, in a sense, "tricked" by the introduction of special numerical boundaries, such as absorbing boundary conditions (ABC's) [11,12] or the perfectly matched layer (PML) [13-16]. ABC's rely on the behavior of a particularly selected differential operator over a spherical surface enclosing the computational domain (the ABC boundary). It can be shown, that an outwardly radiating electromagnetic field can be written in terms of a generalized Wilcox expansion [17] and that the Wilcox basis fields are eigenfunctions of the chosen differential operator, with eigenvalues inversely related to inverse powers of the ABC boundary's radius (i.e., $O(1/r^m)$, m > 0). Thus, the accuracy of this type of method relies not only on the particular radiating field, but on the distance the ABC lies from the source of the radiation [18]. In a sense, the method is also only approximate – regardless of the numerical accuracy with which the electric and/or magnetic fields can be approximated, the ABC does not provide an entirely reflectionless interface for any finite domain.

The PML, on the other hand, serves as the numerical equivalent to pyramidal absorbers in an anechoic chamber. Rather than relying on the shape or any particular numerical trick, the PML can be formulated entirely in terms of material parameters [14]. In theory, if one had access to arbitrary freedom of control over the electric and magnetic parameters of materials, the perfectly matched layer could actually be physically manufactured. Furthermore, in a numerical simulation, if the Maxwell's equations could be solved with infinite discretization accuracy, the PML would be exact – there is theoretically no reflection at the interface between the PML and the medium being matched [19]. The only associated reflection is at the point of termination of the PML layer, but, if designed well, such reflections are typically too small to have a significant impact on the electric field solution. The PML's drawback is in the explicit modeling of fields

within the PML region – such fields are generally not of physical significance to the original open-region problem, but must be discretized by the computational method anyways.

As an alternative, the MoM may be used on the boundary of the domain to divide the problem into two regions: the inhomogeneous region and the free-space region, via the frequency domain electromagnetic surface equivalence principle [19]. The MoM basis functions are used to model electromagnetic currents on the domain boundary which serve as an interface between an open-domain FEM problem and an equivalent closed domain problem. Such a formulation is known as a finite element method/method of moments hybrid method (FEM-MoM) [20]. Of all the methods for domain truncation mentioned here, this one is by far the most exact. The accuracy of the solution in these formulations is not limited by the placement of the boundary or the thickness of an artificial material layer, but merely by the discretization accuracy of the domain itself. The drawback of such methods is the introduction of additional MoM unknowns, and that a MoM discretization results in matrix blocks which are dense, rather than the sparse matrices resulting from pure FEM formulations [21].

Each of these methods has its place in open-domain modeling. They all have relative advantages and disadvantages, and it is up to the user to know how and when each is appropriate to use. However, it is always of interest to continue to develop each of these methods as independent tools, for future students and scientific investigators to use as the world continues to learn more about the topic of electromagnetics. This work is focused around the development of a PML scheme for higher-order finite element methods.

1.3 Goals of the Thesis

The electromagnetics laboratory at the Colorado State University electromagnetics laboratory in the Electrical and Computer Engineering Department is interested in the development and application of fast numerical methods for electromagnetics research and verification. The electromagnetics laboratory maintains two distinct sets of computational codes for the continued development and testing of modern numerical methods. The first of these codes in based upon the electromagnetic Method of Moments (MoM) [21] or Boundary Element Method (BEM), as it is often referred to in literature outside the electromagnetics community. This codes primary purpose utilizes surface discretizations based upon the surface integral equation (SIE) in the electrical field integral equation (EFIE) formulation originating from the electromagnetic surface equivalence principal [19]. The surface of a scatterer or antenna body is discretized by a set of generalized curvilinear quadrilaterals [22], over which a set of basis functions is used to approximate the distribution of equivalent electric and magnetic currents which constitute the boundary between the inside and outside of an equivalent electromagnetic surface.

The second of the computational codes maintained by the electromagnetics laboratory is based upon the FEM. In the FEM code, geometries are primarily discretized using high order polynomial curvilinear elements, over which electric fields are approximated by a high order polynomial basis [23]. This so-called “double higher-order” paradigm of modeling provides a large amount of flexibility over traditional finite element modeling, but presents a unique set of challenges in implementation. The focus of this thesis is on the development of a novel boundary truncation for this code using a conformal PML method [16,24]. While it is often the case that open domain problems in electromagnetics are most often modeled through surface integrals, the

pure finite element method provides a level of flexibility in modeling that cannot be achieved through method of moments formulations based upon surface integral equations. Finite elements easily allow for the approximation of multiple material domains, as well as the modeling of more arbitrary media. Through the introduction of perfectly matched layers, it is hoped that this second computational code can prove just as useful as the first in the area of open region problems.

The conformal perfectly matched layer is an implementation of the PML method of particular interest for the betterment of this second code. Since the FEM has difficutly with accuracy in the area of open-domain modeling, there is much work to be done. By introducing an effective PML method for this code, it may become an excellent tool for comparison to the MoM, and may furthermore be used in the analysis of more exotic devices, where the MoM typically struggles. By using a conformal PML method instead of a more traditional Cartesian or spherical formulation, computational whitespace (the portion of discretized space over which the solutions to Maxwell's equations don't matter) can be minimized.

The primary purpose of this thesis is to develop a fairly automated tool for domain truncation , and to describe the new tool in such a way that future students and researchers in the electromagnetics lab can continue to develop these methods, and to use them freely as tools to advance the future of computational electromagnetics.

1.4 Overview

Chapter 2 of this thesis outlines the theory of the finite element method as it pertains to electromagnetics. In particular, the focus is on the formulation of the double-curl vector wave equation for scattering problems in electromagnetics, and its numerical discretization via

geometrically higher order curvilinear hexahedral elements and a higher order hierarchical curl-conforming basis.

In Chapter 3, an overview of the perfectly matched layer (PML) method is presented, including the historical development of the PML and the variety of different PMLs from electromagnetics literature over the past two decades. The reflectionless characteristic of the PML for the example of a plane wave incident upon a half-space PML is demonstrated via an analytical solution from the viewpoint of elementary electromagnetic theory. Finally, the conformal PML for double higher order finite element methods is presented, including the generation of the PML geometric mesh, the calculation of the corresponding constitutive material parameters, and the optimization algorithm used to improve PML generation for less regular geometries.

In Chapter 4, major changes to the structure and numerical implementation of the higher order finite element code are documented. To serve the ease of implementation of this method and to foster the future development of further numerical methods dependent on this work, a partial overhaul was performed to the associated computational methods. Chapter 4 serves as a description of a subset of important changes to the software either directly or indirectly related to the implementation of the perfectly matched layer. These changes include both structural changes and changes in algorithmic approaches throughout various stages of the finite element analysis.

Chapter 5 presents a variety of numerical examples for the verification of the perfectly matched layer's behavior, and for numerical error comparison to a standard (non-conformal) perfectly matched layer discretization. Simulations based on electromagnetic scattering from

spherical structures are used to quantify error, based on comparisons to analytical methods for scattering analysis. Comparison is made against commercial electromagnetic solvers for numerical examples without analytical solutions. As an example of application within the domain of research, the perfectly matched layer is finally applied to analyze the effectiveness of a spherical cloaking structure based on recent developments in the theory of metamaterials.

Finally, Chapter 6 is used to draw a few remaining conclusions about the successes of this work, comparison to the current state of the art, and potential for future extension. This project leaves multiple possibilities for future work or for further numerical investigations. Additionally, the perfectly matched layer now exists as a tool for the double higher-order finite element method, to aid in electromagnetics research and design for the future.

CHAPTER 2: HIGHER-ORDER FINITE ELEMENTS FOR ELECTROMAGNETIC SCATTERING ANALYSIS

2.1 Background Electromagnetic Theory

The basic fundamental formulation of the finite element method for discretization of the double-curl vector wave equation is presented here. The basis of all electromagnetic theory comes from a set of unified equations written down by James Clerk Maxwell in 1873 [25] known today simply as Maxwell's equations. In modern differential notation, these equations are expressed as [26]

$$\nabla \times \mathbf{E} = -\frac{\partial \mathbf{B}}{\partial t} \tag{2.1}$$

$$\nabla \times \mathbf{H} = \mathbf{J} + \frac{\partial \mathbf{D}}{\partial t} \tag{2.2}$$

$$\nabla \cdot \mathbf{B} = 0 \tag{2.3}$$

$$\nabla \cdot \mathbf{D} = \rho \tag{2.4}$$

Additionally, a set of constitutive material equations relating physical quantities of Maxwell's equations may be expressed as:

$$\mathbf{D} = \overline{\overline{\varepsilon}}_r' \varepsilon_0 \mathbf{E} \tag{2.5}$$

$$\mathbf{B} = \overline{\overline{\mu}}_r \mu_0 \mathbf{H} \tag{2.6}$$

$$\mathbf{J} = \overline{\overline{\sigma}} \mathbf{E} \tag{2.7}$$

The quantities **E, D, H, B,** and **J** are referred to as the electric field, the electric flux density, the magnetic field, the magnetic flux density, and the current density, respectively.

For the purpose of numerical discretization, it is of interest to provide the unification of equations (2.1-2.7) into a single differential equation which describes the spatial and temporal evolution of the electric and magnetic fields. Most often, we are concerned with the time-harmonic solution of equations (2.1-2.7) given a complex sinusoidal excitation. We consider a monochromatic solution, i.e. a solution to Maxwell's equations of the form

$$\underline{\mathbf{E}} = \mathbf{E}_0(x, y, z)e^{-j\omega t}, \underline{\mathbf{H}} = \mathbf{H}_0(x, y, z)e^{-j\omega t} \tag{2.8}$$

Such notation is a mere mathematical convenience – i.e., physical electromagnetic fields are real-valued, measurable quantities, and not complex numbers. However, it is understood that the physically measurable electric and magnetic fields **E** and **H** may be represented as the real part of the phasors in eq. (2.2) Henceforth, the phasor bar notation shall be dropped, and it should be understood that all field variables **E**, **H**, **D**, **B**, and **J** carry with them implicit time dependencies analogous to the form in (2.8). In this notation, equations (2.1) and (2.2) can be rewritten in the frequency domain as [26]

$$\nabla \times \mathbf{E} = -j\omega \mathbf{B} \tag{2.9}$$

$$\nabla \times \mathbf{H} = \mathbf{J} + j\omega \mathbf{D} \tag{2.10}$$

Also of importance in computational methods are the continuity conditions of the electric and magnetic fields at a discontinuity in material parameters. If a surface S_D seperates two

adjacent domains, Ω_1 and Ω_2, and we denote by $\hat{\mathbf{n}}$ the unit normal vector to S_D oriented from Ω_1 to Ω_2, then the continuity conditions which the field variables must satisfy are:

$$\hat{\mathbf{n}}\times\mathbf{E}_1-\hat{\mathbf{n}}\times\mathbf{E}_2=0, \qquad \text{on } S_D \tag{2.11a}$$

$$\hat{\mathbf{n}}\cdot\mathbf{D}_1-\hat{\mathbf{n}}\cdot\mathbf{D}_2=0, \qquad \text{on } S_D \tag{2.11b}$$

$$\hat{\mathbf{n}}\times\mathbf{H}_1-\hat{\mathbf{n}}\times\mathbf{H}_2=0, \qquad \text{on } S_D \tag{2.11c}$$

$$\hat{\mathbf{n}}\cdot\mathbf{B}_1-\hat{\mathbf{n}}\cdot\mathbf{B}_2=0, \qquad \text{on } S_D \tag{2.11d}$$

where the subscript denotes the region in which the field is contained.

Of particular importance is the case of a boundary with a perfect electric conductor (PEC) domain, inside which the electric field and magnetic flux density must vanish. In terms of the boundary conditions (2.11), this implies the familiar boundary conditions

$$\hat{\mathbf{n}}\times\mathbf{E}=0, \qquad \text{on } S_{PEC} \tag{2.12a}$$

$$\hat{\mathbf{n}}\cdot\mathbf{H}=0, \qquad \text{on } S_{PEC} \tag{2.12b}$$

This mathematical nicety is one of the few actual limitations on the propagation of the electromagnetic field. While in reality no such perfect conductor exists, in practice, many materials are impenetrable enough at frequencies of interest (i.e., metals in the microwave regime) to be modeled as such.

By introducing a complex-valued permittivity [26]

$$\bar{\bar{\varepsilon}}_r = \bar{\bar{\varepsilon}}_r' - j\frac{\bar{\bar{\sigma}}}{\omega}, \tag{2.13}$$

equations (1-10) can be combined through simple calculus to produce a single differential vector wave equation [1],

$$\nabla\times\bar{\bar{\mu}}_r^{-1}\nabla\times\mathbf{E}-k_0^2\bar{\bar{\varepsilon}}_r\,\mathbf{E}=0, \tag{2.14}$$

where $k_0=\omega\sqrt{\varepsilon_0\mu_0}$ is the spatial frequency or wavenumber of an electromagnetic wave propagating in free space. These simplifying assumptions allow all the information of Maxwell's equations to be written as a partial differential equation in space in terms of a single field variable **E**. Such a formulation allows us to greatly simplify, since only the electric field **E** has need to be explicitly discretized. Once a solution for **E** is found, equations (2.1-2.6) can be used to find all other field variables. This formulation is known as the double-curl electric field vector wave equation. In a similar manner, we could instead eliminate all field variables from equations (2.1-2.10) except the magnetic field **H** to produce a different single-field formulation, known as the double-curl magnetic field vector wave equation.

For finite element implementation, in an electromagnetic scattering problem, the double-curl equation can be formulated in a more natural manner by decomposing **E** into two parts [19]. We imagine an incident electromagnetic wave $\mathbf{E}^{inc}$ propagating through a vacuum impinging upon a finite region of non-vacuum material. In the absence of the non-vacuum material, such a field must satisfy the wave equation with the material parameters of free space,

$$\nabla\times\nabla\times\mathbf{E}^{inc}-k_0^2\,\mathbf{E}^{inc}=0. \tag{2.15}$$

The scattered electric field $\mathbf{E}^{sc}$ is defined as the difference between the total electric field and a solution to equation (2.15)

$$\mathbf{E}^{sc} = \mathbf{E} - \mathbf{E}^{inc} \tag{2.16}$$

Finally, by subtracting equation (2.15) from (2.14), we arrive at a single differential equation for the unknown scattered field,

$$\nabla \times \bar{\bar{\mu}}_r^{-1} \nabla \times \mathbf{E}^{sc} - k_0^2 \bar{\bar{\varepsilon}}_r \mathbf{E}^{sc} = -\nabla \times (\bar{\bar{\mu}}_r^{-1} - \bar{\bar{I}}) \nabla \times \mathbf{E}^{inc} - k_0^2 (\bar{\bar{\varepsilon}}_r - \bar{\bar{I}}) \mathbf{E}^{inc}, \tag{2.17}$$

where $\bar{\bar{I}}$ denotes the identity tensor.

2.2 Finite Element Discretization

The finite element method (FEM) [27-28] works by the numerical discretization of a differential equation based on the approximation of the solution by an unknown linear combination of basis or "shape" function on a set of subdomains. Suppose the domain of interest is a finite volume of space Ω. We consider a partitioning of the space into N_e subdomains, each of which is called an element. This is illustrated by the two-dimensional domain in Figure 1. The overall computational domain is divided into a series of non-overlapping subdomains. In the case of Figure 1, the domain is tessellated using triangular elements. Triangular tessellations such as this are extremely common in computational methods, due to the large variety of methods for automatic domain triangulation in two or creation of tetrahedral elements in three dimensions, based on Delaunay triangulations [29-30].

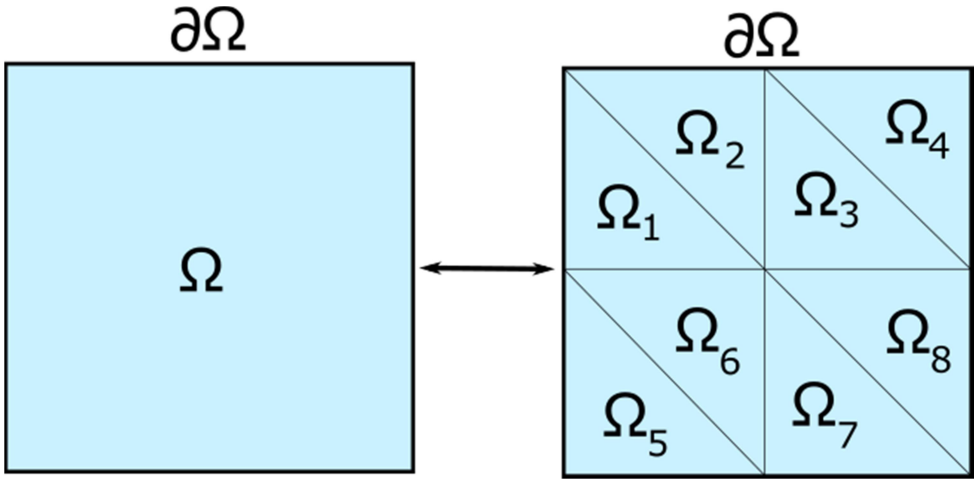

Figure 1. **Division of computational domain into elements:** In the finite element method, the computational domain is divided into subdomains called elements. Here is shown as an example, division of a two-dimensional domain by tessellation with triangles.

In general an element is any of a collection of subdomains Ω_e which partitions the computational domain Ω,

$$\Omega = \bigcup_{e=1}^{N_e} \Omega_e \,,\ \Omega_i \bigcap \Omega_j = \delta_{ij} \Omega_i \,, \tag{2.18}$$

over each of which the unknown variable can be approximated by a linear combination of predetermined basis functions. The flexibility of geometric discretization is one of the biggest strengths of the FEM in computational electromagnetics, as opposed to methods such as the finite-difference time-domain (FDTD) method [9], which must typically be solved on fixed grids. It allows the user to accurately model arbitrary geometries and potentially continuously inhomogeneous and/or anisotropic material properties.

Many forms of geometrical discretization are in practice used to accurately model the shape of the computational domain. By far, the most common form of geometric discretization in computational electromagnetics is through the aforementioned use of tetrahedral elements. Tetrahedral geometric discretization with first-order Nedelec-type edge-based curl-conforming

basis functions [31] is a common standard for discretization of the electric field in electromagnetics, and comprises probably the most common method of finite element discretization for electric fields. Outside of this common modeling paradigm, of particular interest for research is the use of electrically large, curved elements. It has been shown that the use of higher-order basis functions over electrically large elements can lead to increased solution accuracy with a decrease in the number of unknowns present in the system matrix [23]. Instead of the common tetrahedral discretization, a domain can be decomposed using large, arbitrarily-shaped curved generalized hexahedral elements (in three dimensions) or generalized quadrilateral elements (in two dimensions).

The generalized curvilinear hexahedral elements may be described in terms of a mapping from a local cubical domain to their global shape by Lagrange-type interpolatory polynomials. These polynomials allow the user to specify the shape of the element simply by changing the position of a set of interpolation nodes. In general, a single hexahedral element is defined by $(K + 1)^3$ interpolation nodes, where K is the geometrical order of the element. The mapping from a local coordinate system of (u,v,w) to the global position of any point in the element is given by

$$\mathbf{r}(u,v,w) = \sum_{m=0}^{K} \sum_{n=0}^{K} \sum_{l=0}^{K} \mathbf{r}_{mnl} L_k^K(u) L_l^K(v) L_m^K(w), \quad -1 \le u,v,w \le 1. \tag{2.19}$$

Various parameters can be described by use of the local coordinate system (u,v,w), in which the element exists on a cube of edge size 2. The function $L_i^K(x)$ is the i^{th} Lagrange polynomial for a set of K+1 equally spaced interpolation points along the domain $-1 \le x \le 1$, and is given explicitly by the formula

$$L_i^K(x) = \prod_{\substack{l=0 \\ l \neq i}}^{K} \frac{x - x_l}{x_l - x_i}. \tag{2.20}$$

The Lagrange-based interpolatory definition of the element shape is flexible – it allows the user to specify an arbitrary geometrical order for each element (which need not be the same from element to element in a discretization), and it allows the interpolation points to be chosen freely to best fit the geometry and application, and reduces to the simpler and more common geometry of a trilinear hexahedron, or "brick", in the special case of K=1.

The finite element method begins by approximating the electric field distribution on a given element with a set of basis (or "shape") functions. A common higher-order discretization of the scattered electric field may be written as a linear combination of the basis functions over each element up to chosen expansion order (N_u, N_v, N_w) as [23]

$$\mathbf{E}^{\mathrm{sc}} = \sum_{i=0}^{N_u-1}\sum_{j=0}^{N_v}\sum_{k=0}^{N_w} \alpha_{uijk}\,\mathbf{f}_{uijk} + \sum_{i=0}^{N_u}\sum_{j=0}^{N_v-1}\sum_{k=0}^{N_w} \alpha_{vijk}\,\mathbf{f}_{vijk} + \sum_{i=0}^{N_u}\sum_{j=0}^{N_v}\sum_{k=0}^{N_w-1} \alpha_{wijk}\,\mathbf{f}_{wijk} \tag{2.21}$$

The vector basis functions $\mathbf{f}$ are defined in terms of the contravariant basis vectors ($\mathbf{a}^u$, $\mathbf{a}^v$, $\mathbf{a}^w$) of the coordinate transform from the local coordinate system (u,v,w) to the element geometry. Explicitly, they are given in terms of a polynomial basis over a single element

$$\mathbf{f}_{uijk} = u^i P_j(v) P_k(w)\,\mathbf{a}^u \tag{2.22a}$$

$$\mathbf{f}_{vijk} = P_i(u) v^j P_k(w)\,\mathbf{a}^v \tag{2.22b}$$

$$\mathbf{f}_{wijk} = P_i(u) P_j(v) w^k\,\mathbf{a}^w, \tag{2.22c}$$

where $P_n(x)$ is a set of polynomials with the property

$$P_n(x) = \begin{cases} 1-x, & n=0 \\ 1+x, & n=1 \\ n^{th} \text{ order polynomial such that } P_n(-1) = P_n(+1) = 0 & n \geq 2 \end{cases} \tag{2.23}$$

This set of basis functions belongs to the space of curl-conforming functions [32], meaning only the tangential continuity of basis functions is explicitly across element boundaries. This means the electromagnetic boundary conditions between material domains (equations 2.11a-d) can be naturally satisfied if two neighboring elements are constructed of different materials. Additionally, the choice of a curl-conforming basis eliminates the appearance of spurious modes in the solution of eigenvalue problems [32]. For any self-consistent choice of $P_n(x)$ for $n \geq 2$ this set of basis functions is also hierarchical in each of its expansion orders, meaning, e.g., the set of basis functions from choice of order N_u+1 contains the set of basis functions from choice of order N_u as a subset. An analogous statement holds true for N_v and N_w.

A common choice for the high order polynomial basis $P_n(x)$ is the set of modified Legendre polynomials [33], which have the desirable property that they form a nearly orthonormal basis. Explicitly, these polynomials are written in term of the Legendre polynomials as

$$P_n(x) = P_n^L(x) - P_{n-2}^L(x) \qquad n \geq 2 \tag{2.24}$$

where $P_n^L(x)$ is a normalized Legendre polynomial of order n. In all numerical examples of this work, the modified Legendre basis is used.

The curl of the basis functions is also required to calculate a finite element solution, and can be given in terms of the same polynomial basis as

$$\nabla \times \mathbf{f}_{uijk} = \frac{1}{|\mathbf{J}|}[u^i P_j(v) \frac{dP_k(w)}{dw} \mathbf{a}_v - u^i \frac{dP_j(v)}{dv} P_k(w) \mathbf{a}_w]$$

$$\nabla \times \mathbf{f}_{vijk} = \frac{1}{|\mathbf{J}|}[\frac{dP_i(u)}{du} v^j P_k(w) \mathbf{a}_w - P_i(u) v^j \frac{dP_k(w)}{dw} \mathbf{a}_u] \tag{2.25}$$

$$\nabla \times \mathbf{f}_{wijk} = \frac{1}{|\mathbf{J}|}[P_i(u) \frac{dP_j(v)}{dv} w^k \mathbf{a}_u - \frac{dP_i(u)}{du} P_j(v) w^k \mathbf{a}_v]$$

Where $\mathbf{a}_u$, $\mathbf{a}_v$, and $\mathbf{a}_w$ are the covariant basis vectors of the coordinate transform from the unit cube to the element, and $\mathbf{J}$ is the Jacobian matrix of the same transform.

To construct a linear system of equations from the finite element discretization of the electric field, an expression for the residual of the double-curl scattered field wave equation (2.17) is calculated after the geometrical discretization (equations 2.19-2.20) and construction of a proper basis (equation 2.22). Taking the inner product of this residual with a set of testing functions results in a set of linear equations for the unknown coefficients α. Via the Galerkin method, the space of testing functions is chosen to be the same as the basis space.

If a Dirchlet-type boundary condition is enforced on the tangential electric field component across the outer boundary of the computational domain,

$$\hat{n} \cdot \mathbf{E}^{sc} = 0, \text{ on } \partial\Omega, \tag{2.26}$$

then by following this procedure, a standard Galerkin discretization of equation (2.17) is arrived at, as ,e.g. in [28]

$$\int (\nabla \times \mathbf{f}) \cdot \overline{\overline{\mu}}_r^{-1} (\nabla \times \mathbf{E}^{sc}) dV - k_0^2 \int \mathbf{f} \cdot \overline{\overline{\varepsilon}}_r \mathbf{E}^{sc} \, dV = -\int (\nabla \times \mathbf{f}) \cdot \overline{\overline{\mu}}_r^{-1} (\nabla \times \mathbf{E}^{inc}) dV + k_0^2 \int \mathbf{f} \cdot \overline{\overline{\varepsilon}}_r \mathbf{E}^{inc} \, dV \tag{2.27}$$

Without the inclusion of the PML as discussed in chapter 3, or some other form of radiative boundary condition (ABC's, FEM-MoM, etc.), the direct solution to this problem is not representative of the physical electric field.

2.3 Arbitrary Material Parameters

In problems restricted to linear media, the magnetic permeability and electric permittivity functions $\overline{\overline{\mu}}_r$ and $\overline{\overline{\varepsilon}}_r$ relate the values of the electric flux density vector and magnetic field to the electric field and magnetic flux density vector, respectively, as in equations 2.5 and 2.6. The relative magnetic permeability and relative electric permittivity values are often written as scalar functions of the spatial coordinates $\varepsilon_r(x,y,z)$ and $\mu_r(x,y,z)$. However, in their more general form, these values, which serve as linear maps between two vector-valued physical quantities, are symmetric rank-2 tensors. The propagation of electromagnetic waves in arbitrary media may depend on the polarization of the fields or the direction of propagation. Optical birefringence, for instance, is a property often observed naturally in many crystalline materials in which propagation through the material is dependent upon the polarization and propagation direction of incident electromagnetic waves relative to a particular crystal axis [34].

It is also of theoretical interest for the magnetic permeability and electric permittivity tensors to be arbitrary functions of the spatial coordinates within the domain. For instance, deviations in pressure, temperature, and humidity have all been known for long to affect the propagation of radio-frequency electromagnetic waves in the atmosphere [35]. Alternatively, the density of fluids may affect their electromagnetic properties [36], so we may expect, for instance,

gradients in the pressure of seawater, to affect underwater low-frequency wave propagation in a depth-dependent manner.

Outside of purely natural phenomenon, modern manufactured experimental materials regularly feature inhomogeneity and anisotropy. With recent advances in photonics and material sciences, and with the advent of manufacturing and design of metamaterial-based electromagnetic structures, it is easier than ever to manufacture materials with effective bulk material properties which may have behavior well outside the realm of standard isotropic and homogeneous materials. Recently, there has been an active push for the commercialized design of many metamaterial-based electromagnetic components [37]. Microscopic subwavelength features used in metamaterial design are too small to be modeled or to be resolved by electromagnetic waves, but often admit bulk properties as effective anisotropic materials. Spatial variations in micro- and nanofabrication can lead to what is effectively a continuous inhomogeneity in the permittivity and permeability tensors. It is likely that the future of electromagnetic and optical design will involve the computer-aided realization of extremely complex metamaterial devices. This includes the accurate theoretical open-region modeling of electromagnetic devices containing arbitrary media.

Outside of modeling interesting material functions, the PML itself is most commonly formulated as composed of inhomogeneous and/or anisotropic material parameters. Formulating the layer as an anisotropic medium allows suppressed reflection regardless of the direction of incidence, while inhomogeneity is necessary to match interfaces which are not planar. While, the spatial inhomogeneity in a PML is most often approximated, the reflection errors can be greatly reduced if material profiles are modeled smoothly (see section 5.2). It is thus of interest to have

numerical algorithms which are equipped to handle arbitrary anisotropic and inhomogeneous permeability, and permittivity profiles.

We consider the modeling of an arbitrary dielectric function for a device of interest. Continuous inhomogeneity in devices of interest may often be approximated from a macroscopic perspective by piecewise polynomial functions. From a modeling perspective, it is of interest to restrict this type of modeling to polynomials, as step discontinuities are already well-handled by the use of a curl-conforming basis. A Lagrange-type polynomial interpolation scheme is used similar to the geometrical interpolation in equation (2.19). Over a single element, the constitutive material parameters may be smoothly approximated by M^{th} order polynomial interpolation as [38]

$$\overline{\overline{\varepsilon_r}}(u,v,w) = \sum_{m=0}^{M}\sum_{n=0}^{M}\sum_{l=0}^{M}\begin{bmatrix} \varepsilon_{xx} & \varepsilon_{xy} & \varepsilon_{xz} \\ \varepsilon_{xy} & \varepsilon_{yy} & \varepsilon_{yz} \\ \varepsilon_{xz} & \varepsilon_{xz} & \varepsilon_{zz} \end{bmatrix}(u_k, v_l, w_m) L_k^M(u) L_l^M(v) L_m^M(w) \tag{2.28}$$

and

$$\overline{\overline{\mu_r}}(u,v,w) = \sum_{m=0}^{M}\sum_{n=0}^{M}\sum_{l=0}^{M}\begin{bmatrix} \mu_{xx} & \mu_{xy} & \mu_{xz} \\ \mu_{xy} & \mu_{yy} & \mu_{yz} \\ \mu_{xz} & \mu_{xz} & \mu_{zz} \end{bmatrix}(u_k, v_l, w_m) L_k^M(u) L_l^M(v) L_m^M(w), \tag{2.29}$$

where the interpolation points (u_k, v_l, w_m) are $(M+1)^3$ uniformly gridded sampling points along the local element domain $-1 \le u, v, w \le 1$. The material interpolation order M of a particular element can be chosen completely independently of all other elements and of the element's geometrical interpolation order K.

CHAPTER 3: THE PERFECTLY MATCHED LAYER

3.1 Introduction and Background

Boundary conditions in open-domain problems have long been an issue in computational electromagnetics in the use of partial differential equation (PDE) based methods such as the FEM or the FDTD method. When dealing with electromagnetic radiation or scattering problems, effective truncation of the computational domain is a well-investigated problem both in the frequency domain and the time-domain. Various methods such as operator-based absorbing boundary conditions (ABC's) [11-12] and hybrid methodologies based on interfacing with the method of moments (MoM) [1,20-21] have previously been used to effectively terminate the computational domain, but each method has drawbacks.

Rather than applying a specialized boundary condition relying on interfacing with boundary elements (as in the case of a hybrid FEM-MoM) or based on the behavior of a linear differential operator (as in the case of ABC's), the perfectly matched layer (PML) acts effectively as a lossy, impedance matched extension of the regular computational domain. This finite extension contains an additional set of fields (unknowns) which must be explicitly discretized and solved for, and which, when coupled to the fields, mimic the behavior of an infinite, homogeneous, vacuum-filled domain.

A disadvantage of the perfectly matched layer arises from the discretization of the fields within the PML. The value of these fields is generally not of use to the user, merely serving as an effective numerical tool. However, alternative methods almost always lead an increase in the discretized system size. The introduction of extra unknowns into the finite element system of

equations turns out to be a necessary evil for PML implementation, but one which can be dealt with effectively. To minimize this effect, it is advantageous to consider a variety of ways in which this layer can be dealt.

The original perfectly matched layer was formulated an alternative to the traditional ABC in the framework of finite difference time domain simulations by Jean-Pierre Berenger [13]. Berenger's method utilized a splitting of the electric and magnetic fields into multiple components in order to observe the desired effect of a reflectionless, lossy region. Around the same time, Chew and Weedon formulated an alternative version of Berenger's PML from the idea of complex coordinate stretching [14]. They extended the domain of Maxwell's equations from Euclidean space, $\mathbb{R}^3$, onto a complex manifold, $\mathbb{C}^3$. This is accomplished by a modification of the curl and divergence operators to include stretching factors. If these stretching factors are chosen to be complex in the direction normal to an interface, an oscillating solution in an unstretched region of space may be matched to an exponentially decaying oscillation in the stretched space.

Later on, it was shown by Sacks et al. [15] that the perfectly matched layer could be alternatively formulated in Cartesian coordinates as a set of anisotropic material layers. These anisotropic elements can be derived based on phase matching conditions at the interface, and act identically to the complex-coordinate stretching formulation.

3.2 The Perfectly Matched Layer's Behavior

To illustrate the behavior of the PML, we consider the example of a monochromatic plane wave normally incident from free space onto a half-space containing a perfectly matched layer.

A modified, alternate version of Maxwell's equations can be written, as [14]

$$\nabla_s \times \mathbf{E} = -j\omega\mathbf{B} \tag{3.1}$$

$$\nabla_s \times \mathbf{H} = \mathbf{J} + j\omega\mathbf{D} \tag{3.2}$$

$$\nabla_s \cdot \mathbf{B} = 0 \tag{3.3}$$

$$\nabla_s \cdot \mathbf{D} = \rho \tag{3.4}$$

Where the stretched Del operator ∇_s is defined as (in Cartesian coordinates)

$$\nabla_s = \hat{x}\frac{1}{s_x}\frac{\partial}{\partial x} + \hat{y}\frac{1}{s_y}\frac{\partial}{\partial y} + \hat{z}\frac{1}{s_z}\frac{\partial}{\partial z}. \tag{3.5}$$

Here the parameters s_x, s_y and s_z are (generally complex-valued) stretching parameters, which may or may not be coordinate-dependent. Fields which obey these equations are generally "Non-Maxwellian" [16]. That is to say, any set of fields which obeys the differential equations in (3.1-3.5) generally is not representative of a physical set of fields. The parameters s_x, s_y and s_z are generally position-dependent, and the electric and magnetic fields only behave identically to physical fields in limiting case of regions where $s_x = s_y = s_z = 1$, which recovers the situation of the original Maxwell's equations.

We begin by imagining an electromagnetic wave propagating in free space (s = 1) along the z axis, arriving from the negative z direction, polarized entirely along the x axis, incident upon a half-space of PML designed to attenuate waves propagating in the z-direction. Under these simplifications, the stretching variables s_x and s_y can be set to 1, and with a single

remaining stretching variable $s_z=s$ the double-curl vector wave equation in the vacuum can be rewritten as the scalar Helmholtz equation

$$\frac{d}{dz}\frac{1}{\mu_r}\frac{dE_x}{dz}+k_0^2\varepsilon_r E_x=0\,,z<0\,. \tag{3.6}$$

Alternatively, in vacuum, since $\mu_r=\varepsilon_r=1$, this can be rewritten as

$$\frac{d^2E_x}{dz^2}+k_0^2E_x=0\,,z<0\,, \tag{3.7}$$

which has a general electric field solution of the form

$$E_x=E_{inc}e^{-jk_0z}+E_{ref}e^{jk_0z}\,,\ z<0 \tag{3.8}$$

From which a corresponding magnetic field solution can be found using equation (2.9) to be

$$H_y=\frac{E_{inc}}{\eta_0}e^{-jk_0z}-\frac{E_{ref}}{\eta_0}e^{jk_0z}\,,\ \eta_0\equiv\sqrt{\frac{\mu_0}{\varepsilon_0}}\,,z<0 \tag{3.9}$$

Inside the PML region, the field must satisfy the modified Helmholtz equation

$$\frac{1}{s}\frac{d}{dz}\frac{1}{s}\frac{dE_x}{dz}+k_0^2E_x=0\,,z>0 \tag{3.10}$$

which has general solutions of the form

$$E_x=E_{trans}e^{-jk_0sz}\,,\ z>0 \tag{3.11}$$

$$H_y=\frac{E_{trans}}{\eta_0}e^{-jk_0sz}\,,z>0 \tag{3.12}$$

assuming there is no backwards propagating wave in the PML region because the PML medium is unbounded in the positive z direction.

At the division between the two domains, the electric field must satisfy the continuity equations (2.11), which reduces in the one-dimensional case to the continuity of the electric and magnetic fields at the domain boundary, from which the conditions

$$E_{inc} + E_{ref} = E_{trans} \tag{3.13}$$

$$E_{inc} - E_{ref} = E_{trans} \tag{3.14}$$

arise. The only solution that satisfies these conditions simultaneously is the one in which the reflected field is identically zero. The interface shows no reflection.

Furthermore, if the stretching factor s is chosen to be complex valued of the form

$$s = 1 - j\frac{\alpha}{k_0}, \tag{3.15}$$

then the solution inside the PML region decays away from the origin with an exponential factor, explicitly

$$E_x = E_{trans} e^{-jk_0 z} e^{-\alpha z}, z > 0. \tag{3.16}$$

Since the fields decay exponentially inside the PML, the region can be simply truncated after a finite depth, and the interface still results in negligible reflection! For a given choice of alpha, the decay length of the fields inside the PML region can be controlled by the user by varying the parameter α.

A full three dimensional analysis of an arbitrarily oriented reflection from a planar surface can be found in [14]. Any general propagating field may be generally regarded as a superposition of plane waves by Fourier analysis [39] so by analyzing the case of a single arbitrary plane wave, it can be shown that the PML leads to a completely reflectionless interface for any arbitrary propagating (non-evanescent) field.

3.3 The Conformal Perfectly Matched Layer

Several different formulations for the implementation of perfectly matched layers have been presented in literature. These include a variety of Maxwellian [13], Non-Maxwellian [16] formulations, and matching of homogeneous material parameters or general material parameters for dispersive and/or anisotropic materials [40]. The ultimate goal of a PML is to provide an interface for an arbitrary open-domain electromagnetics problem to be terminated, but many of the previously presented PML formulations are for fixed geometrical models. That is, the required interface from the physical domain to the PML domain is required to be one of a few canonical geometries – typically a rectangular prism/cube [14] or a sphere or cylinder [41].

The majority of industrial CEM software provides some manner of built-in PML, but typically only following the modeling paradigm of one of these canonical geometries. For instance, ANSYS, Inc.'s High-Frequency Structure Simulator (HFSS) [42], provides the user only with the option to terminate a domain in a Cartesian PML. COMSOL Multiphysics [43] gives the option to terminate an open domain with either a Cartesian or Spherical PML boundary. It is not difficult to imagine a variety of geometries of interest in which the domain of interest is not particularly representative of a rectangular prism, cylinder, or sphere. For instance, a typical aircraft is significantly wider along its middle section (the wings) and significantly

taller on the tail (the vertical stabilizer) that the rest of the body. Simply attempting to box or put a spherical generates unnecessary computational whitespace which can be avoided by use of a conformal PML.

It is of interest to examine the various PML formulations with respect to the computational requirement. In general the goal of a perfectly matched layer is to reduce the so-called "computational whitespace." That is, the regions of the computational domain which must necessarily be modeled to obtain an accurate system solution, but whose fields are not necessary to calculate a quantity of interest (QoI). For example, the Kirchoff integral formulation (see section 3.6) allows one to calculate the electric and magnetic fields anywhere outside of the computational domain if they are known entirely on a surface completely enclosing a scattering body [19]. It is thusly ideal for a computational program to solve explicitly for the fields in as little of the air-filled domain as possible.

In the past, there have been a variety of attempts to formulate a conformal PML. A PML layer which conforms as closely as possible to the geometry of interest clearly presents the best computational option for PML generation, because in the case of arbitrary geometry, it minimizes the amount of this computational whitespace. The most common formulation for a conformal PML [41] relies on a local orthogonal coordinate system and the calculation of local Darboux frames at the PML boundary. The problem with such an implementation is that in the case of sharp regions of the mesh ("corners"), the principle curvatures of the mesh are singular, and these local frames cease to be well-defined.

The conformal PML can also be compared to some alternate domain truncation methods in terms of its computational efficiency and accuracy. The first method of interest primarily used

to truncate the computational domains in the codes of interest was a hybrid formulation with the method of moments. While the FEM-MoM hybrid method [20] accomplishes the goal of domain truncation with great accuracy, it requires the additional implementation of a set of divergence-conforming basis functions (representative of electric and magnetic currents) over the surface enclosing the exterior of the computational domain. The overall number of unknowns in the system of equations arising from the FEM-MoM is thus generally fewer than the discretization utilizing a PML, but the block of the matrix representing coupling between MoM basis functions is completely dense. The high computational cost of solving for unknowns from a dense matrix block can outweigh the benefits of reducing the system size, so generally such a formulation is not always desirable.

Alternatively, the first-order ABC based on a generalized Wilcox expansion provides a fairly straightforward method to, but with accuracy dependent on the distance of the boundary from the scattering body [11]. Extension to a second-order ABC requires the numerical computation of the divergence of basis functions [12], and with a curl-conforming basis, the divergence of these functions may be singular at element edges, so special care must be taken to not introduce additional error into the computation. While a properly implemented second-order ABC may overcome some of the problems of the first order, and furthermore, are known to be less accurate for arbitrary angles of incidence.

The conformal PML then serves as a good alternate to the aforementioned methods. The formulation for a finite element method based upon double higher-order scattering analysis is based mostly upon the locally-conformal formulation of the stretched-coordinate PML introduced by Ozgun and Kuzuoglu [16]. The locally-conformal PML consists of several element layers of with directly calculated modified curl operators based on the notion of complex

coordinate stretching. The PML of this work, however, only consists of a single layer of geometrically curved artificial anisotropic media. The goal is to generate an anisotropic PML layer around an existing mesh, and to generate the appropriate material. It is assumed that a convex mesh of a scattering body exists, including a surrounding air cushion layer. The convexity of the inner mesh is already a necessary requirement for the PML to behave correctly, so although this may prove an inconvenience for odd arbitrarily-shaped geometries it is a necessary computational expense.

It is worth noting that there have been attempts based around PML methods to allow truncation of domains with concave regions, both by transformation electromagnetics methods [44], and by specially constructed PML layers [45] but such approaches are so far uncommon and/or incomplete and generally beyond the scope of this thesis. This is left for a possible open problem in future development of the involved computational electromagnetics codes.

In the PML formulation for scattering computation, the domain Ω is partitioned into three disjoint domains, as in Figure 2. The innermost domain $\Omega_{SCATTERER}$ is filled with scattering bodies made of general dielectric inhomogeneous and/or anisotropic materials. It may also include perfectly conducting bodies, which are modeled only by their surface $\partial\Omega_{PEC}$, over which the appropriate boundary condition (equation 12) can be enforced. Around the scattering body is a vacuum-filled domain Ω_{AIR}. A portion of the air domain, typically around .3 free space wavelengths in thickness, must be explicitly meshed to maintain accuracy of the PML method. Surrounding the air domain is the PML region Ω_{PML}. The boundary separating the region Ω_{AIR} from Ω_{PML} is also of importance and is denoted by $\partial\Omega_{PML}$. Finally, the outer boundary of the computational domain is denoted by $\partial\Omega$.

With the inclusion of the PML in the computational domain, the solution of the scattered field double-curl electric field wave equation may be fully cast as a boundary value problem:

Find $\mathbf{E}^{sc}$ such that

$$\nabla \times \bar{\bar{\mu}}_r^{-1} \nabla \times \mathbf{E}^{sc} - k_0^2 \bar{\bar{\varepsilon}}_r \mathbf{E}^{sc} = \mathbf{g}(\mathbf{r}), \tag{3.17}$$

subject to the boundary conditions

$$\mathbf{n} \cdot \mathbf{E}^{sc} = 0 \text{ on } \partial\Omega \tag{3.18a}$$

$$\mathbf{n} \cdot \mathbf{E}^{sc} = -\mathbf{n} \cdot \mathbf{E}^{inc} \text{ on } \partial\Omega_{PEC}, \tag{3.18b}$$

and where the excitation function $\mathbf{g}(x)$ is defined as a piecewise function in terms of the incident electric field

$$\mathbf{g}(\mathbf{r}) = \begin{cases} -\nabla \times (\bar{\bar{\mu}}_r^{-1} - \bar{\bar{I}}) \nabla \times \mathbf{E}^{inc} - k_0^2 (\bar{\bar{\varepsilon}}_r - \bar{\bar{I}}) \mathbf{E}^{inc} & \mathbf{r} \in \Omega_{SCATTERER} \\ 0 & otherwise \end{cases}. \tag{3.19}$$

The first step of PML implementation is to generate a geometrical model of the conformal PML domain Ω_{PML} given a higher order geometrical mesh of a scattering body and its convex hull. This can be accomplished via a method of projections. At each geometrical node on the surface of a given mesh, the unit normal to the surface is calculated. The direction of the normal to a face of an element is given by the appropriate contravariant (dual) basis vectors ($\mathbf{a}^u$, $\mathbf{a}^v$, $\mathbf{a}^w$). These basis vectors are in turn calculated in terms of the covariant (primary) basis vectors ($\mathbf{a}_u$, $\mathbf{a}_v$, $\mathbf{a}_w$) and the Jacobian $\mathbf{J}$ of the local-to-global coordinate transformation of the element as [18]

$$\mathbf{a}^u = \frac{\mathbf{a}_v \times \mathbf{a}_w}{|\mathbf{J}|} \tag{3.20}$$

$$\mathbf{a}^v = \frac{\mathbf{a}_w \times \mathbf{a}_u}{|\mathbf{J}|} \tag{3.21}$$

$$\mathbf{a}^w = \frac{\mathbf{a}_u \times \mathbf{a}_v}{|\mathbf{J}|} \tag{3.22}$$

The Jacobian is the ratio of the differential volume of the hexahedral to the differential volume of the unit cube, and can be calculated for arbitrary coordinate systems simply as the volume of the parallelepiped formed by the primary basis vectors.

$$|\mathbf{J}| = \mathbf{a}_w \cdot (\mathbf{a}_u \times \mathbf{a}_v) = \mathbf{a}^w \cdot (\mathbf{a}^u \times \mathbf{a}^v) \tag{3.23}$$

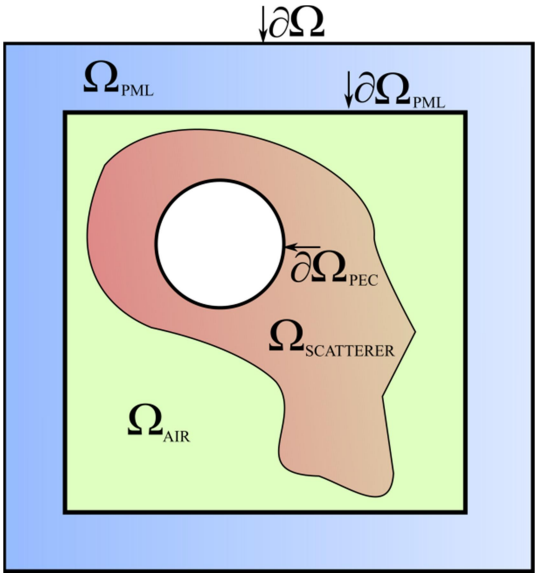

Figure 2: Domain Divison. With the use of a PML, the computational domain is divided into three distinct regions. The innermost region consists of dielectric scattering bodies and possibly perfect electrically conducting surfaces. Surrounding that is a region of free space/air, which provides and shapes the domain into a convex shape for interfacing with the PML region. Finally, the domain is truncated in a PML layer with an outer Dirichlet-type boundary condition.

The primary basis vectors ($\mathbf{a}_u$, $\mathbf{a}_v$, $\mathbf{a}_w$) are first calculated by derivatives of the coordinate system with respect to the local-to-global mapping (2.19). These vectors are geometrically tangent vectors to the planes of constant *u, v,* or *w.* Their formulas are given by

$$\mathbf{a}_u = \frac{\mathrm{d}\,\mathbf{r}}{\mathrm{du}} \tag{3.24a}$$

$$\mathbf{a}_v = \frac{\mathrm{d}\,\mathbf{r}}{\mathrm{dv}} \tag{3.24b}$$

$$\mathbf{a}_w = \frac{\mathrm{d}\,\mathbf{r}}{\mathrm{dw}}. \tag{3.24c}$$

These derivatives are most efficiently calculated after a change of basis in equation (2.19) has been made. After the Lagrange interpolatory basis has been constructed, the mapping from the local cube element to its geometry can be rewritten as

$$\mathbf{r} = \sum_{k=0}^{K}\sum_{l=0}^{K}\sum_{m=0}^{K}\hat{\mathbf{r}}_{klm}u^k v^l w^m \ . \tag{3.25}$$

From this, the primary basis vectors at a position (u,v,w) are given by

$$\mathbf{a}_u = \sum_{k=1}^{K}\sum_{l=0}^{K}\sum_{m=0}^{K}\hat{\mathbf{r}}_{klm}(k-1)u^{k-1}v^l w^m, \tag{3.26a}$$

$$\mathbf{a}_v = \sum_{k=0}^{K}\sum_{l=1}^{K}\sum_{m=0}^{K}\hat{\mathbf{r}}_{klm}(l-1)u^k v^{l-1} w^m, \tag{3.26b}$$

$$\mathbf{a}_w = \sum_{k=0}^{K}\sum_{l=0}^{K}\sum_{m=1}^{K}\hat{\mathbf{r}}_{klm}(m-1)u^k v^l w^{m-1}. \tag{3.26c}$$

It is important to note that the primary and dual basis vectors are not necessarily of unit length. After calculation of the dual basis vectors at every node of interest on an element face, they are normalized to calculate a normal unit vector $\hat{n}$.

From the normal of each node on the surface a new set of nodes is calculated. To generate an M^{th} order geometrical PML element, M new nodes are generated for each surface node at positions

$$\mathbf{r}_i = \mathbf{r}_{projection} + i\frac{\hat{n}t_{PML}}{M}, i \in 1,2,...M \tag{3.27}$$

where $\mathbf{r}_{projection}$ is the node on the surface, and t_{PML} is the user-specified PML layer thickness. For each element face which exists on the PML boundary $\partial\Omega_{PML}$, these nodes are then connected to form a new element.

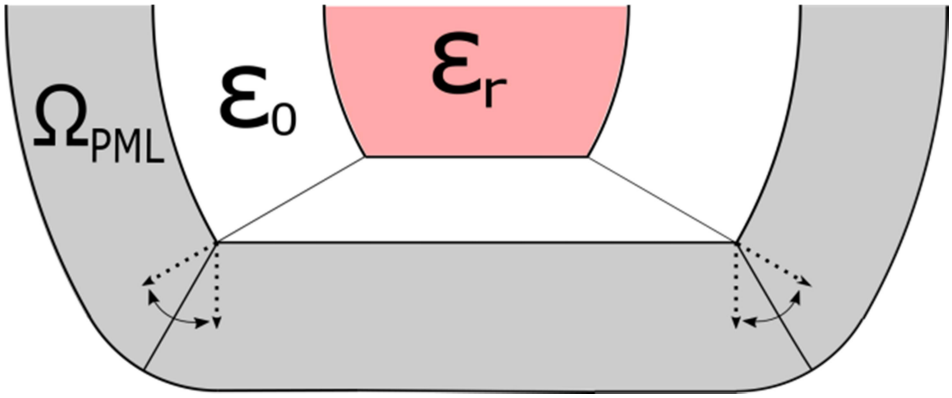

Figure 3. Projection of Elements: Surface normal vectors are calculated at the nodal interpolation points on the PML boundary to create PML elements by outward projection. At corner areas where nodes may be shared by multiple element faces, the surface normal vectors are averaged to create a projection direction.

Some of the nodes exist on the edges or corners of elements, in which case they may be shared by multiple elements or multiple faces of the same element on $\partial\Omega_{PML}$. In this case multiple normal vectors are calculated for a single (one normal vector to each boundary face constructed from that node). While these normal vectors will not generally be oriented in the same direction, they can be averaged to calculate an approximate normal vector along which the new nodes can be calculated.

The process of normal averaging is illustrated for part of an arbitrarily shaped, curved 2D mesh in Figure 3. For the nodes corresponding to corners of the mesh during the PML element generation, there are multiple normal vectors to the different faces. These normal vectors are averaged to calculate a direction of projection.

Because large, curvilinear elements are being used, it suffices in most applications to generate just a single element per face on the boundary. A typical choice for PML thickness is in terms of the free-space wavelength, about $.3\lambda_0$ [44].

3.4 Stretching Function for the Conformal PML

After the generation of the elements in the PML, as detailed in Section 3.3, the appropriate permeability and permittivity tensor functions must be generated in a systematic way to ensure that the PML acts as a lossy material and that the boundary conditions for zero wave reflection across the air/PML interface are satisfied. Following the precedent set by Chew and Weedon [14] and followed by many subsequent implementations, the behavior of the conformal PML is formulated in terms of the complex coordinate-stretching approach. This conformal PML implementation is generated via a spatial transformation based upon the locally-conformal formulation of the stretched-coordinate PML introduced by Ozgun and Kuzuoglu [44].

The complex coordinate transform which leads to the desired behavior is the one which stretches (in a complex manner) each point directly away from the closest point on the air/PML boundary. To each point P in a given PML element with position $\mathbf{r}$, there is a unique point P_0 on the boundary $\partial\Omega_{PML}$ with position $\mathbf{r}_o$ satisfying

$$\mathbf{r}_0 = \min_{\mathbf{r} \in \partial\Omega_{pml}} \|\mathbf{r} - \mathbf{r}_0\| \tag{3.28}$$

The uniqueness of the point P_0 is guaranteed by the constraint that $\partial\Omega_{PML}$ must necessarily be convex. It has been previously shown that the convexity of the air/PML boundary is already necessary condition to guarantee the proper behavior of the PML [45].

Once each PML material interpolation point P has been mapped back to the closest point P_0 on the PML boundary, it is stretched away from the PML domain by the complex mapping:

$$\tilde{\mathbf{r}} = \mathbf{r} - \frac{j}{k_0} f_1(\|\mathbf{r} - \mathbf{r}_0\|) \frac{(\mathbf{r} - \mathbf{r}_0)}{\|\mathbf{r} - \mathbf{r}_0\|} + \frac{1}{k_0} f_2(\|\mathbf{r} - \mathbf{r}_0\|) \frac{(\mathbf{r} - \mathbf{r}_0)}{\|\mathbf{r} - \mathbf{r}_0\|} \tag{3.29}$$

This flexible stretching function generalizes the constant factor s used to demonstrate the PML behavior in section 3.2. In this transformation, are two separate stretching factors. The first of these creates a real-to-complex coordinate transformation which casuses the exponential decay of propagating electromagnetic waves. The second, real, stretching factor creates a virtual thickening of the PML domain for non-propagating (evanescent) electromagnetic waves, which helps to attenuate them more effectively. The spatial transformation in equation (3.29) is illustrated in Figure 4 for an arbitrarily shaped mesh in two dimensions.

The requirement on the stretching functions $f_i(\|\mathbf{r} - \mathbf{r}_0\|)$ is that they be monotonically increasing functions of the distance from the PML boundary. The class of polynomial functions

$$f_i(\|\mathbf{r}-\mathbf{r}_0\|) = \alpha_i \|\mathbf{r}-\mathbf{r}_0\|^p \tag{3.30}$$

satisfies the required monotonicity [16]. For the remainder of this work it shall be assumed that, unless explicitly stated otherwise, the PML stretching function is a first-order (linear) function of the distance from the PML/air boundary ($p = 1$).

From the complex coordinate transformation in equation (3.29), each node in Ω_{PML} is mapped to a new position $\tilde{\mathbf{r}}$. A new Lagrange interpolation is calculated from these nodal points for each element, which can be expressed after a basis change in the (u,v,w) polynomial basis as

$$\tilde{\mathbf{r}} = \sum_{k=0}^{K}\sum_{l=0}^{K}\sum_{m=0}^{K} \hat{\tilde{\mathbf{r}}}_{klm} u^k v^l w^m \ . \tag{3.31}$$

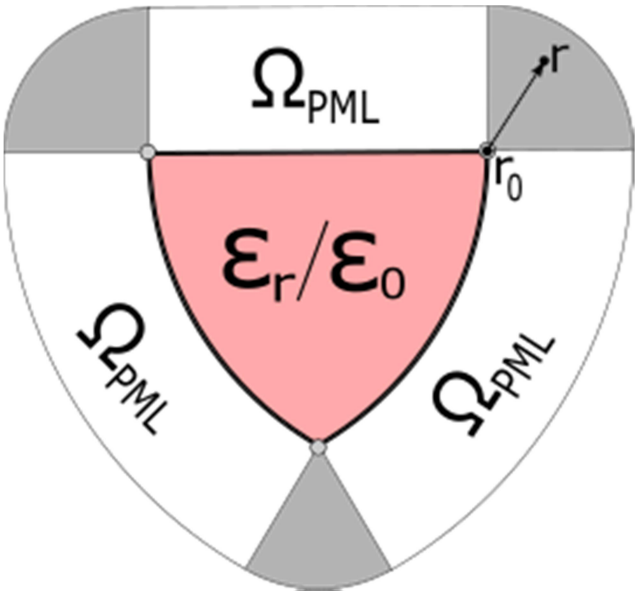

Figure 4. Complex Coordinate Stretching. Each point within the PML domain is mapped back to a point on the PML boundary, which it is stretched away from. In the dark shaded regions, the closest points on the PML boundaries are the corners, so all points in a given shaded section will be stretched away from the same corner point.

As has been well studied, Maxwell's equations exhibit certain invariance under coordinate transformations. Maxwell's equations on a modified coordinate system may be written to have the same formal appearance as the original frequency-domain Maxwell's with alternate material tensors. Such an idea forms the basis or an entire body of work in transformation optics/electromagnetics theory [46].

Utilizing theory from transformation optics, we can generate new material parameters which recover the form of the unmodified Maxwell's equations in the PML domain, but with modified material constituent tensors

$$\tilde{\bar{\bar{\varepsilon}}}_r = \frac{\tilde{\mathbf{J}}^T \bar{\bar{\varepsilon}}_r \tilde{\mathbf{J}}}{\left|\tilde{\mathbf{J}}\right|}, \qquad \tilde{\bar{\bar{\mu}}}_r = \frac{\tilde{\mathbf{J}}^T \bar{\bar{\mu}}_r \tilde{\mathbf{J}}}{\left|\tilde{\mathbf{J}}\right|} \tag{3.32}$$

Here, the Jacobian $\tilde{\mathbf{J}}$ is the transformation from the coordinate-stretched space back to the original space.

$$\tilde{\mathbf{J}} = \frac{\partial \mathbf{x}}{\partial \tilde{\mathbf{x}}} = \begin{bmatrix} \frac{\partial x}{\partial \tilde{x}} & \frac{\partial x}{\partial \tilde{y}} & \frac{\partial x}{\partial \tilde{z}} \\ \frac{\partial y}{\partial \tilde{x}} & \frac{\partial y}{\partial \tilde{y}} & \frac{\partial y}{\partial \tilde{z}} \\ \frac{\partial z}{\partial \tilde{x}} & \frac{\partial y}{\partial \tilde{y}} & \frac{\partial y}{\partial \tilde{z}} \end{bmatrix} \tag{3.33}$$

By application of the chain rule for partial derivatives, the Jacobian can be written in terms of the local-to-global geometrical Jacobians as

$$\tilde{\mathbf{J}} = \tilde{\mathbf{J}}_{\text{elem}}^{-1} \mathbf{J}_{\text{elem}} \tag{3.34}$$

$$\mathbf{J}_{\text{elem}} = \frac{\partial \mathbf{x}}{\partial \mathbf{u}}, \tilde{\mathbf{J}}_{\text{elem}} = \frac{\partial \tilde{\mathbf{x}}}{\partial \mathbf{u}}. \tag{3.35}$$

3.5 Optimization for the Conformal PML

Due to the projection process described in Section 3.3, every point **r** within the PML has a point of origin $\mathbf{r}_{\text{projection}}$ on the surface of the PML boundary from which it was projected, which would be the closest point to it on the PML boundary, $\mathbf{r_0}$, if the projection was calculated using true normal vectors. However, due to the averaging of normal vectors at nodes shared by one or more elements, the projection point $\mathbf{r}_{\text{projection}}$ may be not be the point which satisfies the condition (3.28). This introduces a problem, because failure to satisfy this condition leads to an imperfectly matched boundary and extra numerical reflections.

To overcome the difficulty of exact minimization, it is useful to implement a quick numerical optimization algorithm to eliminate any errors imposed by the projection process. For a given material interpolation point P with position **r** and element ε from which it was projected, the cost function to be minimized is

$$f_c(u,v,w) = \left\|\mathbf{r} - \mathbf{r}_0(u,v,w)\right\|^2, \ \mathbf{r}_0 \in \Omega_\varepsilon \tag{3.36}$$

This cost function can be minimized numerically by means of a constrained gradient descent algorithm [47]. To ensure the true global minimum of this function is found, the gradient descent is evaluated to find the closest point in all elements from which it was projected. For instance, if a surface node is shared at the intersection of 4 elements, all PML nodes projected from it will need to be optimized back to those 4 elements. The gradient descent is evaluated separately using each of these elements, and then the minimum of those points is taken to be the true global minimum of (3.28).

For each optimization, the algorithm begins with an initial point $(u,v,w)_0$ such that $\mathbf{r}_0(u,v,w)_0 = \mathbf{r}_{\text{projection}}$. The algorithm repeatedly updates the initial point based on the gradient of the cost function

$$(u,v,w)_{k+1} = (u,v,w)_k - \beta \nabla f_c(u,v,w)\gamma^k \tag{3.37}$$

The factor β is a constant which is dependent upon the absolute scale of the problem, and the factor γ^k is included to ensure faster convergence of the algorithm in the case of possible oscillations around a local minimum. For practical purposes, a choice of around γ=.9 ensures sufficiently rapid convergence.

Explicitly, the gradient of the cost function can be given in terms of the basis vectors in the element ε

$$\nabla f_c(u,v,w) = 2\begin{bmatrix} [\mathbf{r}-\mathbf{r}_0(u,v,w)]\cdot \mathbf{a}_{u,0}(u,v,w) \\ [\mathbf{r}-\mathbf{r}_0(u,v,w)]\cdot \mathbf{a}_{v,0}(u,v,w) \\ [\mathbf{r}-\mathbf{r}_0(u,v,w)]\cdot \mathbf{a}_{w,0}(u,v,w) \end{bmatrix}. \tag{3.38}$$

The update of position is is also constrained at every step to stay within the local coordinate cube

$$-1 \le u_k, v_k, w_k \le 1 \tag{3.39}$$

by projecting the vector $(u,v,w)_k$ back onto the cube anytime one or more of the conditions in (3.39) is violated.

The algorithm is set to terminate for each node if the absolute update in position is below a selected tolerance τ, that is, if

$$\left\|\mathbf{r}(u_k,v_k,w_k) - \mathbf{r}(u,v,w)\right\|^2 < \tau\,. \tag{3.40}$$

3.6 Calculation of Quantities of Interest

The radar cross section is a common way to quantify the scattering of electromagnetic fields. Once the electric field is known within the computational domain, assuming that the infinite space surrounding the physical problem is filled with a homogeneous medium, the scattered field anywhere can be analytically calculated at an arbitrary point in space. If a closed surface S_{FF} can be drawn which encloses entirely a region of non-vacuum materials, the electric field anywhere outside the surface can be calculated using the free space electromagnetic Green's function formalism. The integral which expresses the scattered electric field at an arbitrary position $\mathbf{r}$ as a function on the electric fields on S_{FF}, is commonly known as the Kirchoff integral [1],

$$\mathbf{E}^{sc}(\mathbf{r}) = \oint_{S_{FF}} \{\hat{n}' \times [\nabla' \times \mathbf{E}(\mathbf{r}')] G(\mathbf{r},\mathbf{r}') + [\hat{n}' \times \mathbf{E}(\mathbf{r}')] \times \nabla' G(\mathbf{r},\mathbf{r}') + [\hat{n}' \cdot \mathbf{E}(\mathbf{r}')] \nabla' G(\mathbf{r},\mathbf{r}')\} dS', \tag{3.41}$$

where the free space Green's function $G(\mathbf{r},\mathbf{r}')$ is

$$G(\mathbf{r},\mathbf{r}') = \frac{1}{4\pi \|\mathbf{r}-\mathbf{r}'\|} e^{-jk_0\|\mathbf{r}-\mathbf{r}'\|} \tag{3.42}$$

The bistatic radar cross section of an object at a single frequency is defined in terms of spherical coordinates as

$$\sigma(\theta_{inc},\phi_{inc},\theta_{sc},\phi_{sc}) = \lim_{r\to\infty} 4\pi r^2 \frac{\left|\mathbf{E}^{sc}(r,\theta_{sc},\phi_{sc})\right|^2}{\left|E_0\right|^2} \tag{3.43}$$

This quantity describes the percentage of electromagnetic power scattered in a particular direction (normalized to be invariant over distance), and depends both on the direction of

incidence (radar source position) and the direction of observation (radar receiver position). Most often the radar cross section is expressed in a normalized form in a decibel scale [19],

$$\sigma_{Normalized} = \lim_{r\to\infty} 10\log_{10}\left(\frac{4\pi r^2}{\lambda_0^2}\frac{\left|E^{sc}\right|^2}{\left|E^{inc}\right|^2}\right). \tag{3.44}$$

In the Fraunhofer (far-field) limit [48], the scattered field must transform into a propagating plane wave, meaning only the transverse components of the electric and magnetic fields contribute to far off scattered fields. The third term in (3.41) vanishes in this limit and

$$\mathbf{E}^{sc}(\mathbf{r}) = \frac{e^{-jk_0 r}}{4\pi r}\oint_{S_{FF}}\left\{\hat{n}'\times[\nabla'\times\mathbf{E}(\mathbf{r}')] + jk_0[\hat{n}'\times\mathbf{E}(\mathbf{r}')]\times\frac{\mathbf{r}}{r}\right\}dS' \tag{3.45}$$

which can be used for far-field calculations. Here, r = |**r**|, the distance of the observation point.

The near-to-far-field transformation surface S_{FF} can be any closed surface completely enclosing the scattering body. For PML implementation, it suffices to use the PML boundary $\partial\Omega_{PML}$, with the integration using the value of the fields directly on the *inside* of the surface (that is, the air elements).

The integral in equation (3.41) can be evaluated using either the scattered or total field on the surface S_{FF}, since the incident plane wave itself cannot contribute to a scattered field [18]. Thus, the calculation of the radar cross section does not vary significantly in the new scattered field formulation from the previous formulation.

CHAPTER 4: DETAILS ON SOFTWARE IMPLEMENTATION

4.1 Parallelization

In the modern world of scientific computing, algorithms must be efficiently parallelizable in order to be competitive. Amdahl's law [49] dictates that the most fundamental limitation on the speed of a modern computer program is the percentage of the computation which is parallelizable, so it is of significant interest to identify the most computationally expensive aspects of, and exploit any parallelism available.

Of particular interest for targeted parallelization are the most numerically intensive sections of the finite element discretization. By far the most computationally expensive part of the finite element solution is in the solution of the resulting linear system of equations. Previously, the linear system solution was handled by the parallel sparse solver PARDISO as part of the Intel Math Kernel Library [50], operating primarily on desktop workstations. The PARDISO package solves the system of equations simultaneously for all right-hand sides using a direct forward and backward substitution [51].

Computing the monostatic radar cross-section of a particular target can become extremely computationally expensive with regards to the number of right-hand sides. To achieve a full 3D cross section with a solid angle resolution of, e.g. 1 square degree, requires over 3000 separate right-hand side vectors. While Krylov subspace-based iterative methods [52] are often the most efficient method for discretization based on particularly high frequency problems and scale better in computational time with the number of unknowns [1], for moderately sized systems of equations direct solvers can prove to be the best option, particularly with a large

number of right-hand side vectors. Whereas iterative methods must be restarted for each unique excitation, Gaussian elimination-based factorization methods can reduce a system of equations for all right-hand sides simultaneously. Direct solutions also provide a robustness that cannot be matched in an iterative solver – failure of convergence is not an issue, nor is the choice of an appropriate preconditioner.

For nondefinite complex linear systems, the PARDISO solver provides routines for shared memory architectures using OpenMP directives to distribute the workload over multiple cores of the same machine. This is somewhat unsatisfactory from a software engineering perspective, as it severely limits the size of problem which can be simulated using this type of direct solution.

Instead, the MUltifrontal Massively Parallel Sparse Direct Solver (or MUMPS) library is one of several standards in high-performance computing for parallel computation of direct solution to sparse systems of equations. The MUMPS solver is available as part of the Cray PETSc [53] suite on Colorado State University's Cray high-performance computing system [54], and is easily callable through an interface with Fortran 90. It employs the Message Passing Inteface (MPI) standard for interprocess communication [55]. MUMPS works on an algorithm known as the multifrontal factorization algorithm. Different processes in a multifrontal solver operate on different "fronts" (blocks of data based on a precomputed symbolic factorization tree), performing limited steps of standard Gaussian elimination so as to avoid a large number of fill-ins to the system matrix.

The second largest computational draw of the software is in the assembly of the entries in the system matrix itself. Higher order finite elements exhibit a trade-off between a reduced

system size [18] and more complicated assembly. Whereas in a low order finite element method, the assembly of each individual element is a quick computation, in a high order method, the element geometry, basis functions, material parameters, etc., may all be high order polynomials. and in order to calculate an accurate system matrix, a high order accuracy quadrature rule must be used. To make efficient use of multiple processes, the assembly workload must be efficiently distributed across the available resources. A single element with, e.g., electric field approximation order of N_u=N_v=N_w=8 can have a local (dense) matrix of size 1944x1944. Furthermore, since the system matrix is formed from a set of dense local calculations, the overall system matrix has a strongly block-diagonal structure, which is extremely appropriate for frontal elimination.

Because of the elemental structure of the matrix, the assembly portion of the computational code is somewhat simple to parallelize. A simple heuristic algorithm is used to distribute the elemental structures over the pool of processes. The number of required calculations for each element is calculated based on the elements' local matrix size and quadrature order. A cumulative sum of the number of computations is then calculated for all elements in order, and then the elements are distributed in chunks to processes in order, in a manner such that the i^{th} process receives as to $N_{computations}/p$ as possible, where $N_{\text{computations}}$ is the total number of cumulative computations over matrix filling for all elements, and p is the number of processes over which the workload is distributed.

4.2 Excitation Vector Filling

In the switch from a total field formulation to a scattered field formulation, the manner in which the excitation vector is calculated requires changes in implementation. In the standard

total field formulation, there must also be included a surface integral (boundary term) over the entirety of the computational domain resulting from the variational formulation [18]. This surface integral can be used to interface with differential operator-based absorbing boundary conditions. However, with the PML, the domain is terminated with Dirchlet-type boundary conditions at the outer edge instead, so the boundary term is nonexistent. Instead, the wave equation is written in terms of separate scattered and incident fields. The form of the incident field is assumed to be known. The most typical incident field can be represented by a plane wave. In the Fraunhofer or far-field limit [48], as the separation of the wave source and observation point increases without bound, all propagating electromagnetic fields can be viewed as effectively plane waves.

A plane wave propagating through free space takes the general form

$$\mathbf{E}^{inc}(\mathbf{r}) = E_0 e^{-j\mathbf{k}\cdot\mathbf{r}}\hat{E}, \tag{4.1}$$

where the wave vector **k** has the direction of propagation of the plane wave and a magnitude equal to k_0, and the electric field polarization vector $\hat{E}$ is always orthogonal to **k**. The user provides the direction of arrival in terms of spherical coordinates. The spherical coordinate convention of choice is to denote by θ the elevation angle and by ϕ the azimuthal angle, with θ measured from 0 at the positive z-axis. The direction of incidence is specified as the direction from which the plane wave is arriving by the elevation and azimuthal angles of arrival, θ_{inc} and ϕ_{inc}. We define a rotated orthonormal frame, composed of the unit vectors.

$$\hat{r}_{inc} = sin\,\theta_{inc}\cos\phi_{inc}\,\hat{x} + \sin\theta_{inc}\sin\phi_{inc}\,\hat{y} + \cos\theta_{inc}\,\hat{z}, \tag{4.2a}$$

$$\hat{\theta}_{inc} = \cos\theta_{inc}\cos\phi_{inc}\,\hat{x} + \cos\theta_{inc}\sin\phi_{inc}\,\hat{y} - \sin\theta_{inc}\,\hat{z} \tag{4.2b}$$

$$\hat{\phi}_{inc} = -\cos\theta_{inc}\sin\phi_{inc}\,\hat{x} + \cos\theta_{inc}\cos\phi_{inc}\,\hat{y} - \sin\theta_{inc}\,\hat{z} \tag{4.2c}$$

which are constant, and are defined to be equal to the standard spherical unit vectors evaluated in the direction of $\hat{r}_{inc}$. these, the wave vector has the value

$$\mathbf{k} = -k_0\hat{r}_{inc}, \tag{4.3}$$

and the electric field can be rewritten as.

$$\mathbf{E}^{inc}(\mathbf{r}) = E_\theta e^{-j\,\mathbf{k}\cdot\mathbf{r}}\hat{\theta}_{inc} + E_\phi e^{-j\,\mathbf{k}\cdot\mathbf{r}}\hat{\phi}_{inc} \tag{4.4}$$

It is often of interest to explicitly specify the amplitudes of the field with respect to the spherical basis, E_θ and E_ϕ, because most modern radar systems are typically designed to maintain electromagnetic isolation between two perpendicularly polarized transmitter channels. As an example, polarimetric radar systems for weather can be used to determine other quantities of interest based on multiple polarization cross sections such as the differential reflectivity [56].

From (4.4), the curl of the incident field can be written in the form

$$\nabla\times\mathbf{E}^{inc}(\mathbf{r}) = -j\left(\mathbf{k}\times\hat{E}\right)E_0 e^{-J\,\mathbf{k}\cdot\mathbf{r}} = -jk_0(E_\theta\hat{\phi}_{inc} - jk_0E_\phi\hat{\theta}_{inc})e^{-J\,\mathbf{k}\cdot\mathbf{r}}, \tag{4.5}$$

from which the excitation vector can be quickly filled using a predetermined quadrature rule.

CHAPTER 5: NUMERICAL SIMULATIONS

5.1 Effect of Material Function on Solution Error

For validation of numerical methods in computational electromagnetics, it is of interest to simulate scattering problems which admit analytical or closed-form solutions. Due to the complex nature of open-region problems in 3 dimensions, few finite domains admit solutions with exactly calculable radar cross-sections. One of the canonical geometries to admit an easily computable analytical solution for numerical comparison is that of plane wave scattering from a dielectric or perfectly electrically conducting sphere in the form of Mie's series [19].

The spherical symmetry allows the problem to be reduced to a series of one dimensional problem by a change of basis. A generally oriented (scalar) plane wave may be expanded via a wave transformation as

$$e^{i\mathbf{k}\cdot\mathbf{r}} = \sum_{l=0}^{\infty} (2\ell+1) i^{\ell} j_{\ell}(kr) P_{\ell}(\hat{\mathbf{k}}\cdot\hat{\mathbf{r}}) \tag{5.1}$$

where the functions $j_{\ell}(x)$ are lth order spherical Bessel functions of the first kind and P_{ℓ} are the Legendre polynomials. Scattering for each of these spherical waves can easily computed by application of the proper material interface boundary conditions (equations 2.11). In practice, such a series must always be computed for a finite number of terms, and the precision may be improved by adding more terms to the series. The full details of computation for the Mie's series can be found in many graduate electromagnetics textbooks [19], but are used here for the quantification of absolute accuracy in numerical simulation of scattering bodies.

In particular, it is of interest to isolate and examine that numerical error which is caused by the ability of a method to accurately approximate the necessary material parameters. Generally, matching a PML to any non-Cartesian geometry will require anisotropic material parameters which vary continuously. Failure to accurately model these material parameters leads to increased discretization error, and the behavior of the PML degrades as a result.

The spherical example to be examined is composed of 15,317 2nd order geometrical model, with a discretization chosen so that the edge length of all elements is not to exceed λ/10, where

$$\lambda = \frac{\lambda_0}{\sqrt{\varepsilon_r \mu_r}} \tag{5.2}$$

is the wavelength of electromagnetic waves within the dielectric medium of the scattering sphere. Additionally, the fields within each element are expanded in terms of third-order polynomial basis functions, $N_u = N_v = N_w = 3$. The use of 3rd order field approximation ensures this example is very over-refined, in order to isolate the error caused by the material parameter approximation from geometrical modeling errors and errors caused from a lack of mesh refinement.

The sphere is electrically of a medium size, with a .5m radius and a relative permittivity value of $\varepsilon_r = 2.25$. The models are surrounded first by a .3m thick spherical shell of air and then by a .3m thick PML layer with a Dirichlet-type boundary at the outside radius to terminate the computational domain.

Two models are compared to the Mie's series solution in terms of their absolute accuracy – in the first model, the material parameters are modeled as piecewise constant values based on

exact evaluation of the material functions in spherical coordinates, computed at the local center ($u = v = w = 0$) of each element. In the other, the material parameters are calculated during meshing from the process described in Section 3.4 and approximated via 2nd order Lagrange-type interpolatory polynomials (M = 2).

The absolute errors in the radar-cross section compared to the Mie series as computed from the two models are plotted in Figure 5. A drastic reduction in the numerical error is seen from using the optimized and continuously inhomogeneous PML parameters. Across the range of azimuthal angles, there is a decrease in the reflection error by a factor of 10 to 100.

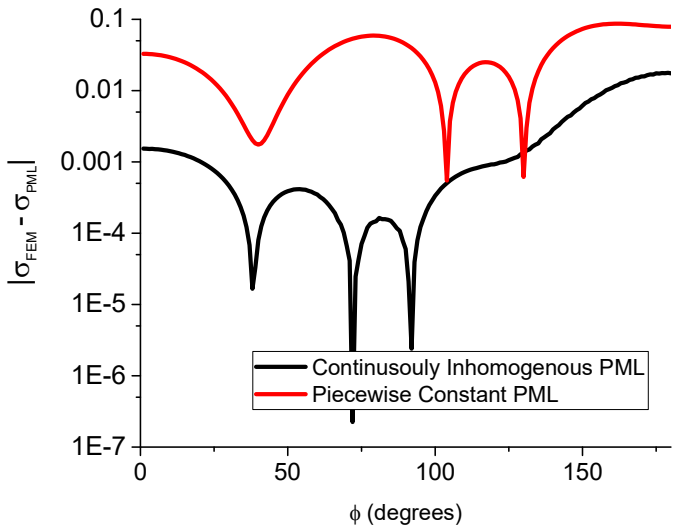

Figure 5: Material Discretization Comparison: The absolute error in bistatic radar cross section is computed for a spherical dielectric scatterer using the PML for curvilinear higher-order finite element discretization. The solution error is compared to a typical PML discretization using piecewise. The model is otherwise well over-refined, both in a geometrical sense, and in terms of the electric field approximation error, so as to isolate the PML's error from other sources of discretization error.

Even with a piecewise constant material function, the PML does a remarkably good job in providing an accurate termination of the computational domain. However, this example shows that the accuracy of modeling the relevant material parameters clearly serves as a limiting factor to the accurate computation of radar cross-sections. It has been well known that the main cause of PML inaccuracy is due to discretization error [19], but there have so far been relatively few PML implementations proposed which overcome this limitation.

5.2 Radar Cross Section of Almond Scatterer

The NASA almond was proposed as one of a series of benchmarks for the development and verification of computational electromagnetic scattering software [57]. It was initially proposed as a physically manufacturable target for testing the accuracy of radar cross-section measurements [58], but later adapted one of several standard test cases for numerical methods in electromagnetics. The shape of an almond provides a simple, but interesting benchmark for the validation of numerical methods due to its diversity in geometrical features. At the back end, an almond is round, providing a smooth surface. However, the tip of an almond is quite sharp, converging to a single point in front.

The shape of the almond is described in terms of a set of parametric equations describing the surface geometry. Every cross section of the almond perpendicular to its longest axis (the x-axis) is elliptical with a width 3 times wider than its height. End to end, the entire almond measures $d = 9.936$ inches, and its surface can be parametrized in two parts in terms of variables t and ψ.

$$x = dt$$

$$y = .193333d\sqrt{1-\left(\frac{t}{.416667}\right)^2}\cos\psi \qquad -.41667 < t < 0, -\pi < \psi < \pi \tag{5.3a}$$

$$z = .064444d\sqrt{1-\left(\frac{t}{.416667}\right)^2}\sin\psi$$

$$x = dt$$

$$y = 4.83345d\left[\sqrt{1-\left(\frac{t}{2.08335}\right)^2} - .96\right]\cos\psi \qquad 0 < t < .58333\,, -\pi < \psi < \pi \tag{5.3b}$$

$$z = 1.61115d\left[\sqrt{1-\left(\frac{t}{2.08335}\right)^2} - .96\right]\sin\psi$$

While the NASA almond appears most frequently in literature as a metallic shape (most appropriate for computational methods based on surface discretization, such as the method of moments), its general geometry also provides a useful benchmark for the investigation of dielectric scattering bodies. We use the almond geometry as a useful comparison for the PML in the case where the mesh exhibits features other than the perfect roundness of a spherical scatterer.

Since the almond does not present an analytical solution for its radar cross-section, an alternate method of accuracy verification needs to be used. The electromagnetic solver WIPL-D is based upon the MoM method in the surface integral equation formulation, and is used to compare the field solution with the PML based FEM. Comparison against a completely different computational method such as this serves as good verification of accuracy. The computed bistatic radar cross section of the NASA almond is plotted in Figure 6 against the cross section computed from WIPL-D. The incident field is z-polarized, propagating from the +z direction

toward the tip of the almond. Good agreement is seen between the MoM solution and the FEM with PML.

Additionally, the real, z-directed component of the scattered electric field is plotted in Figure 7 for the z = 0 cross section of the almond to provide a visual comparison. In the top figure (FEM), the fields are shown for the entire computational domain including the air layer. Very little computational whitespace is needed in this problem, as the almond shape serves as its own convex hull. The decay of the fields in the PML region is immediately visible.

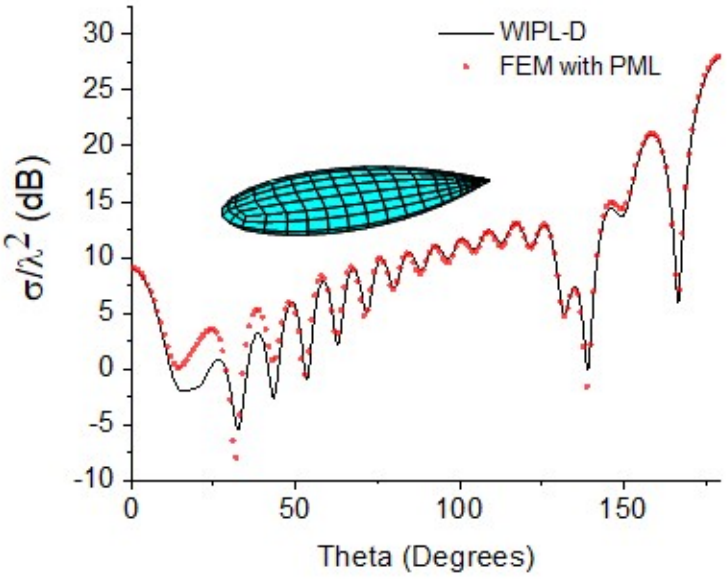

Figure 6. NASA Almond Bistatic Cross Section Comparison: The bistatic radar cross section of a dielectric NASA almond computed from the FEM is compared against a commercial solver WIPL-D. Good agreement is seen between the two solutions

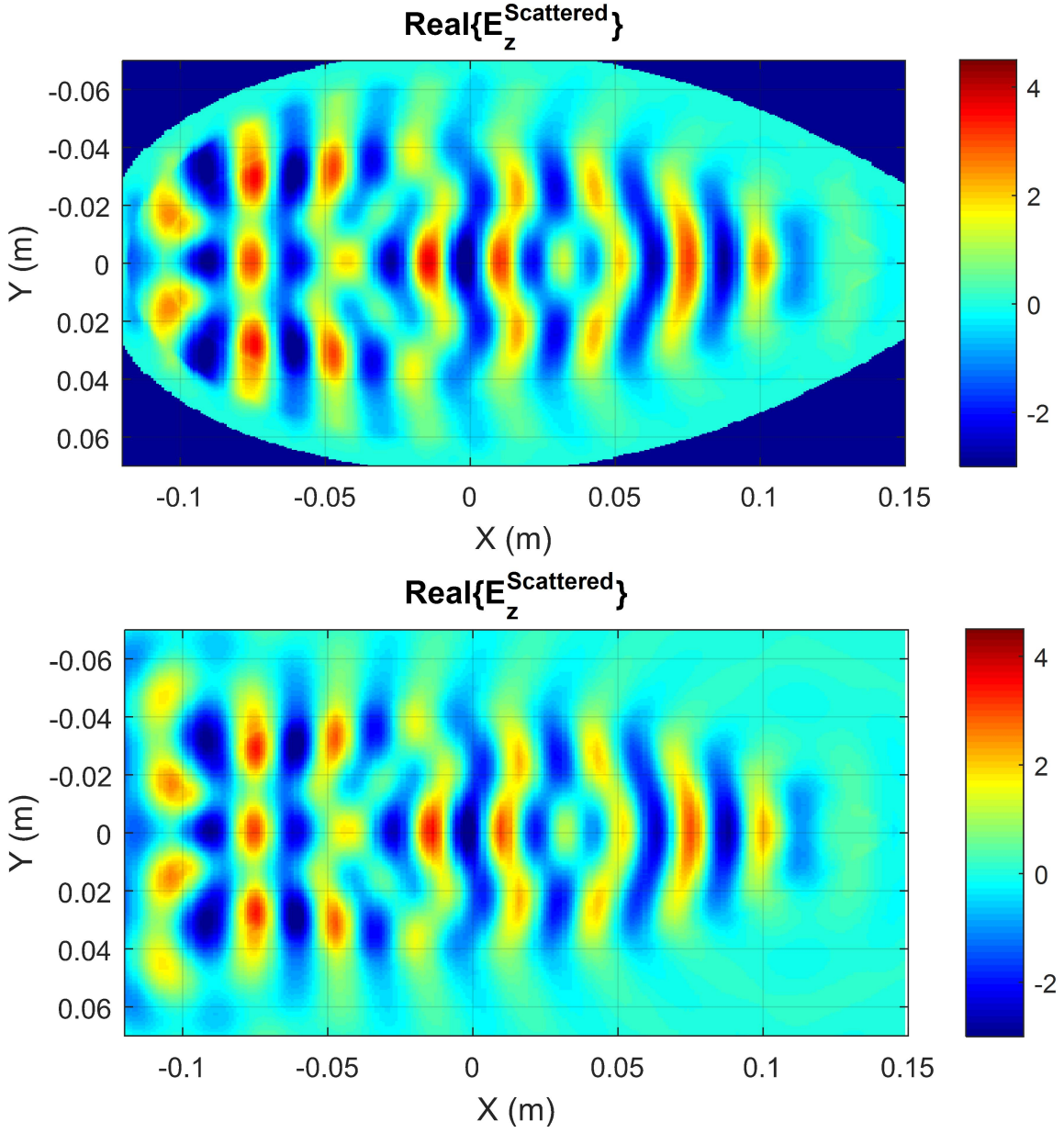

Figure 7. Comparison of NASA Almond Near Field Solutions: Top: Real, z-directed scattered electric field component calculated from finite element scattering solution of NASA almond. Bottom: Calculated from MoM surface discretization using WIPL-D.

5.3 Spherical Metamaterial Cloaking Structure

A substantial research interest has grown in recent years in the design and manufacturing of metamaterials [37]. At radio frequencies, resonant structures based upon split ring resonator geometries in effect provide engineered bulk material properties which may appear continuously inhomogeneous and/or anisotropic [59]. One of the canonical examples of the metamaterial manufacturing dream is the design of an electromagnetic invisibility cloak – an object which is completely undetectable by electromagnetic waves at particular frequencies. One can easily imagine applications of such a device in radar countermeasure technology or in antennas designed to minimize the effects on interference from certain frequency bands. In practice, such a cloak can be approximately designed, but only for fairly small frequency bands, since metamaterials usually rely upon the resonant behaviors of electrically small subwavelength structures. Experimental demonstrations of this sort of resonant behavior often come up in the field of plasmonics [60], in which frequencies close to the natural resonant frequency of electrons in a metal cause the metal of exhibit a virtually negative index of refraction at certain optical frequencies.

The behavior of the original electromagnetic cloak was described in a theoretical formalism in terms of ray optics [61]. Based on the ideas of transformation electromagnetics, a change in material parameters can be viewed as causing an identical behavior to a distortion in the coordinate system of a space. It was shown that an arbitrarily chosen inhomogeneous propagation medium can be used to essential steer electromagnetic energy in a free manner. In fact, this same idea forms the basis for the ability to express the stretched-coordinate PML formulation as a set of inhomogeneous constitutive material parameters (see Section 3.4).

Previously, a higher-order spherical cloak was simulated using continuously inhomogeneous material parameters based on the FEM-MoM hybrid formulation to deal with the open-domain boundary conditions [62]. Here, a dielectric sphere with diameter of 3λ and a relative permitivitty of $\varepsilon_r = 2.25$, is simulated surrounded completely by a metamaterial cloak. The cloak is based on a linear mapping function, and consists entirely of an inhomogeneous layer only 2 elements thick. The appropriate material parameters are approximated by 4^{th} order interpolations.

Figure 8 shows the normalized bistatic cross section calculated from the entire device, compared to the Mie's series solution. We see a reduction of the cross section to less than -50 dB around the entirety of the sphere. Figure 9 shows the real, z-directed component of the total electric field in and around the dielectric sphere. The incident waves are in essence bent completely around the sphere, and the electric field inside the dielectric is reduced to near zero.

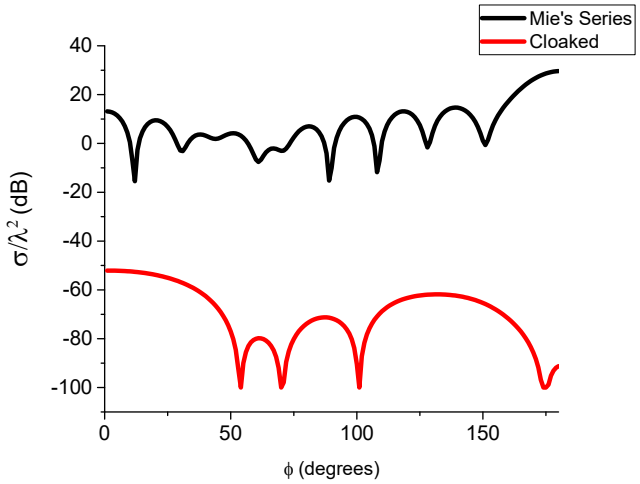

Figure 8. Spherical Cloak Normalized Bistatic Cross Section: An inhomogeneous, anisotropic cloaking structure is placed around, and the finite element method is used to calculate the (normalized) bistatic radar cross section. The bistatic radar cross-section is compared to the analytical solution for scattering from an uncloaked sphere. The cloak reduces the radar cross-section of the sphere to less the -50dB throughout the entirety of the azimuthal plane.

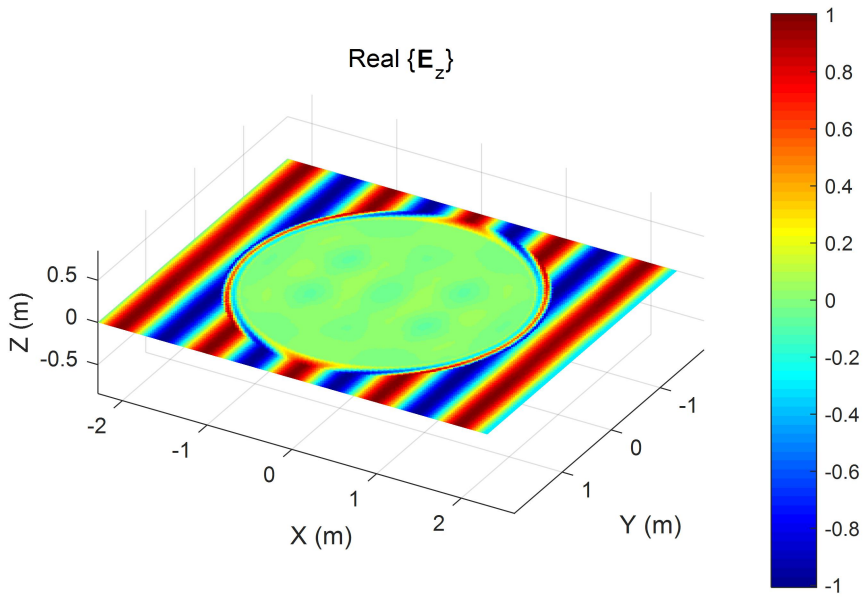

Figure 9. Spherical Cloaking Device Electric Field Cut: A snapshot of the total electric field (z-component) in the near-field of an electromagnetic cloaking device. The exotic material parameters surrounding a dielectric sphere effectively bend an incident plane wave around the scattering body. The plane wave propagation exhibits only minimal disturbance by the presence of the entire structure.

CHAPTER 6: CONCLUSION

6.1 Conclusions and Future Work

The perfectly matched layer is an effective and accurate method of terminating the unbounded domain arising in electromagnetic scattering problems modeled using higher order finite elements. Based on the Lagrange-type interpolated geometry, a method of conformal PML generation is studied for use with higher-order curvilinear finite element methods. Surface normals are calculated from the geometrical mesh, and are used as guides for a complex-coordinate stretching approach to PML implementation. This formulation differs fundamentally from a typical conformal PML method, in which local orthogonal coordinate systems based on Darboux frames are used to generate material parameters. A modified gradient descent algorithm is presented to correct any error in the generated material parameters arising from errors in the geometrical discretization.

Numerical results support the conclusion that the implementation of a conformal perfectly matched layer in the higher order FEM modeling paradigm provides benefits over traditional PMLs with piecewise constant material parameters, with the reflection error in a spherical dielectric scatterer example being reduced by a factor of 10 to 100 using the higher order material approximations inherent to the new method. The ability of the new anisotropic locally-conformal higher order PML to accurately and efficiently analyze scatterers with a large variation in geometrical shape is demonstrated in an example of a dielectric almond, which is challenging for PML modeling because of the sharp tip and round back, as well as the tapered shape of the almond. The performance of the method in analysis of objects with unconventional and challenging to model material compositions is demonstrated via an example utilizing a

spherical continuously inhomogeneous and anisotropic cloaking structure based on transformation optics.

This work represents only a fraction of the total possibilities for development of the perfectly matched layer for higher order curvilinear finite element methods in electromagnetics. There are still many possible investigations to be done in the development of this boundary condition. Additional numerical experimentation on the effects of PML parameters on solution accuracy can be done to determine the optimal choice of the stretching function for. Possibly parameters of interest to investigate include the degree of the polynomial stretching function used to calculate the PML material parameters, the coefficients of the PML stretching function, and the effects of geometric curvature on the accuracy of the PML. Additionally, this work has potential use to be extended to methods for PML generation and analysis in the time-domain.

This work is a first step toward automated PML generation for curvilinear hexahedral elements in higher order finite element methods for electromagnetics. Further investigation will hopefully help quantify the effects of all parameters on the PML's accuracy and eventually be able to automate the entirety of PML generation and use.

REFERENCES

[1] J.-M. Jin, *Finite Element Analysis of Antennas and Arrays*, 1st ed., US, Hoboken, NJ: John Wiley & Sons, 2009

[2] F. Pedrotti, L. M. Pedrotti, and L. S. Pedrotti, *Introduction to Optics*, 3rd ed., Pearson, 2006

[3] J. S. Asvestas, "The physical optics method in electromagnetic scattering," *Journal of Mathematical Physics*, vol. 21, pp. 290, 1980

[4] L. Greengard and V. Rokhlin, *"*A fast algorithm for particle simulations," *Journal of Computational Physics*, vol. 73, pp. 325-348, 1987

[5] J. D. Jackson, *Classical Electrodynamics*, 3rd ed., Wiley, 1998

[6] N. M. Newmark, "A method of computation for structural dynamics," *J. Eng. Mech. Div. Proc. Am. Soc. Civil Eng.*, vol. 85, pp. 67–94, July 1959.

[7] O. Pironneau, *Finite Element Methods for Fluids*, Universite Pierre et Marie Curie & INRIA, 1988

[8] J. N. Reddy, D. K .Gartling, *The Finite Element Method in Heat Transfer and Fluid Dynamics*, 3rd ed, US: New York, CRC Press, 2010

[9] K. S. Yee, "Numerical solution of initial boundary value problems involving Maxwell's equations in isotropic media," *IEEE Trans. Antenn. and Propag.,* vol. AP-14, pp. 302–307, May 1966

[10] V. Rodriguez, "Basic Rules for Anechoic Chamber Design, Part One: RF Absorber Approximations", *Microwave Journal*, vol. 59, pp. 72-84, 2016

[11] A. Chatterjee and J. Volakis, "Conformal absorbing boundary conditions for 3-D problems: derivation and applications," *IEEE Transactions on Antennas and Propagation,* vol. 43, No. 8, August 1995, pp. 860-866

[12] B. Engquist and A. Majda, "Absorbing boundary conditions for the numerical simulation of waves," *Math. Comp.* vol. 31, 1977, pp. 629-651

[13] J. P. Berenger, "A perfectly matched layer for the absorption of electromagnetic waves," *J. Comput. Phys*., vol. 114, pp. 185-200, Oct. 1994.

[14] W. C. Chew and W. H. Weedon, "A 3D perfectly matched medium from modified Maxwell's equations with stretched coordinates*," Microw. Opt. Technol. Lett*., vol. 7, pp. 599-604, Sept. 1994.

[15] Z. S. Sacks, D. M. Kingsland, R. Lee, and J.-F. Lee, "A perfectly matched anisotropic absorber for use as an absorbing boundary condition," *IEEE Trans. Antennas Propag*., vol 43, pp. 1460-1463, Dec.1995.

[16] O. Ozgun and M. Kuzuoglu, "Non-Maxwellian locally-conformal PML absorbers for finite element mesh truncation," *IEEE Trans. Antennas Propag*., vol. 55, pp. 931-937, 2007.

[17] C. H. Wilcox, "An expansion theorem for electromagnetic fields," *Commun. Pure Appl. Math.,* vol. 9, pp. 115-132, 1956.

[18] M. M. Ilic, *Higher Order Hexahedral Finite Elements for Electromagnetic Modeling*, US: UM Dartmouth, 2003

[19] J.-M. Jin, *Theory and Computation of Electromagnetic Fields*, 2nd ed., US, Hoboken, NJ: John Wiley & Sons, 2015

[20] M. M. Ilic, M. Djordjevic, A. Z. Ilic and B. M. Notaros, "Higher order hybrid FEM-MoM technique for analysis of antennas and scatterers", *IEEE Transactions on Antennas and Propagation,* vol. 57, No. 5, 2009

[21] R. F. Harrington, *Field Computation by Moment Methods,* 1st ed, US: Wiley-IEEE Press, reprinted 1993

[22] M. Djordevic and B. M. Notaros, "Double Higher Order Method of Moments for Surface Integral Equation Modeling of Metallic and Dielectric Antennas and Scatterers," *IEEE Transactions on Antennas and Propagation,* vol. 52, no. 8, 2004

[23] M. M. Ilic and B. M. Notaros, "Higher Order Hierarchical Curved Hexahedral Vector Finite Elements for Electromagnetic Modeling", *IEEE Trans. on Microwave Theory and Techniques,* vol. 51, no. 3, 2003, pp. 1026-1033

[24] F. L. Teixeira and W. C. Chew, "Analytical derivation of a conformal perfectly matched absorber for electromagnetic waves," *Microw. Opt. Technol. Lett.,* vol. 17, pp. 231–236, March 1998

[25] J. C. Maxwell, *A Treatise on Electricity and Magnetism,* 3rd ed., vol. 1. New York: Dover, 1954

[26] B. M. Notaros, *Electromagnetics*, 1st ed., USA, NJ, Upper Saddle River: Prentice-Hall, 2011

[27] K. W. Morton and D. Mayers, *Numerical Solution of Partial Differential Equations*, New York: Cambridge University Press, 1st ed., 2005

[28] J.-M. Jin, *The Finite Element Method in Electromagnetics,* 2nd Ed., US, New York: John Wiley & Sons, 2002

[29] D. T. Lee and B. J. Schachter, Two Algorithms for Constructing a Delaunay Triangulation, *Int. Jour. of Comp. and Inform. Sciences,* Vol. 9, No. 3*,* 1980, pp. 219-242

[30] P. J. Frey and P.-L. George, *Mesh Generation: Application to Finite Elements*, 2nd ed., US, Hoboken, NJ: John Wiley & Sons, Inc.

[31] J. C. Nedelec, "Mixed finite elements in R3," *Numer. Math.,* vol. 35, pp. 315-341, 1980.

[32] R. D. Graglia, D. R. Wilton, and A. F. Peterson, “Higher order interpolatory vector bases for computational electromagnetics,” *IEEE Transactions on Antennas and Propagation*, Vol. 45, No. 3, March 1997, pp. 329-342.

[33] M. M. Ilić and B. M. Notaroš, “Higher order large-domain hierarchical FEM technique for electromagnetic modeling using Legendre basis functions on generalized hexahedra,” *Electromagnetics*, vol. 26, pp. 517–529, Oct. 2006.

[34] http://www.olympusmicro.com/primer/lightandcolor/birefringence.html, “Optical Birefringence,” Accessed 6/22/17

[35] E. K. Smith, Jr., and S. Weintraub, “The Constants in the Equation for Atmospheric Refractive Index at Radio Frequencies,” *Proceedings of the I.R.E.,* 1953, pp. 1035-1037

[36] B. B. Owen et. al., “The Dielectric Constant of Water as a Function of Temperature and Pressure”, *Journal of Physical Chemistry,* vol. , 1961, pp. 2065-2070

[37] A. Alù, "Metamaterials: Prime time." *Nature Materials*, vol. 15, pp. 1229-1231, Nov. 2016.

[38] M. M. Ilic, A. Z. Ilic, B. M. Notaros, “Continuously Inhomogeneous Higher Order Finite Elements for 3-D Electromagnetic Analysis,” vol. 57, 2009, pp. 2798-2803

[39] J. W. Goodman, *Introduction to Fourier Optics*, 3rd ed., US: W. H. Freeman, 2004

[40] S. D. Gedney, “An anisotropic PML absorbing media for the FDTD simulation of fields in lossy and dispersive media,” *Electromagn.,* Vol. 16, pp. 399-415, 1996.

[41] F. L. Teixeira and W. C. Chew, “Systematic Derivation of Anisotropic PML Absorbing Media in Cylindrical and Spherical Coordinates,” *IEEE Microw. Guided Wave. Lett.*, vol. 7, pp. 371-373, Nov. 1997.

[42] ANSYS, Inc., “HFSS: Perfectly Matched Layer Boundary Automation”, online, 2016. Accessed June 23, 2017.

[43] COMSOL Multiphysics “Comsol Blog: Using Perfectly Matched Layers and Scattering Boundary Conditions for Wave Electromagnetics Prolems,” online. January 28, 2015. Accessed June 23, 2017.

[44] O. Ozgun and M. Kuzuoglu, “Domain Compression via Anisotropic Metamaterials designed by Coordinate Transformations,” *Journal of Computational Physics,* vol. 229, no. 3, pp. 921-932 2010.

[45] K. Sainath and F. L. Teixeira, “Perfectly reflectionless omnidirectional absorbers and electromagnetic horizons,” *JOSA B*, vol. 32, no. 8, pp. 1645-1646.

[46] A. J. Ward and J. B. Pendry, “Refraction and geometry in Maxwell’s equations,” *J. Modern. Optics*, vol. 43, pp. 773-793, 1996

[47] E. K. Chong and S. H. Zak. *An introduction to optimization*. John Wiley & Sons, 2013

[48] J. Mertz, *Introduction to Optical Microscopy*, 1st ed. USA: Roberts and Company, 2009.

[49] M. Quinn, *Parallel Programming in C with MPI and OpenMP,* 1st ed, McGraw-Hill Science, 2003

[50] Intel, *Intel Math Kernel Library: Developer Reference,* revision 76, MKL 11.3, online, accessed June 23, 2017

[51] *Pardiso User Guide Version 5.0.0*, online, Version 5.0.0, accessed June 23, 2017

[52] R. Barrett, et. al, *Templates for the Solution of Linear Systems: Building Blocks for Iterative Methods*, 2nd ed: SIAM, 1994

[53] Argonne National Laboratory, *PETSc Users Manual*, Revision 3.7. Online, accessed June 23, 2017.

[54] Colorado State University Information Science and Technology Center, *ISTeC Cray High Performance Computing System: User's Guide*, Version 5.2. online, accessed June 23, 2017.

[55] *MUltifrontal Massively Parallel Solver (MUMPS 5.1.1) Users' Guide*, March 21, 2017, online, accessed June 23, 2017.

[56] C. Kleinkort, et. al. "3D Shape Reconstruction of Snowflakes from Multiple Images, Meshing, Dielectric Constant Estimation, Scattering Analysis, and Validation by Radar Measurements." *American Meteorological Society's 37th Conference on Radar Meteorology*, 14-18 September, 2015, Norman, OK.

[57] J. Volakis, "Benchmark Radar Targets for the Validation of Computational Electromagnetics Programs," *EM Programmer's Notebook, IEEE Antennas and Propagation Magazine,* vol. 35, No. 1, 1993.

[58] A. K. Dominek, H. T. Shamanski, R. Wood, and R. Barger, "A Useful Test Body," in *Proceedings Antenna Measurement Techniques Association,* September 24, 1986.

[59] R. Marques, et. al., "Left-Handed-Media Simulation and Transmission of EM Waves in Subwavelength Split-Ring-Resonator-Loaded Metallic Waveguides", *Physical Review Letters,* vol. 89, no. 18, 2002

[60] S. A. Maier, *Plasmonics: Fundamentals and Applications,* 1st ed, USA: New York, Springer Science + Business Media LLC, 2007.

[61] J. B. Pendry, D. Schurig, D. R. Smith, "Controlling Electromagnetic Fields." *Science,* vol. 312, pp. 1780-1782, 2006.

[62] S. V. Savić, A. B. Manić, M. M. Ilić, B. M. Notaroš, "Efficient Higher Order Full-Wave Numerical Analysis of 3-D Cloaking Structures", *Plasmonics*, pp. 455-463, 2013.

APPENDIX A: PUBLICATIONS OF THE AUTHOR

Journal Papers

[1] A. B. Manic, A. P. Smull, F-H. Rouet, X. S. Li, and B. M. Notaros, "Efficient Scalable Parallel Higher Order Direct MoM-SIE Method with Hierarchically Semiseperable Structures for 3D Scattering", *IEEE Trans. Antennas and Prop.,* pp. 2467-2478, Vol. 65, 2017

[2] A. P. Smull, A. B. Manic, S. B. Manic, and B. M. Notaros, "Anisotropic Locally-Conformal Perfectly Matched Layer for Higher-Order Curvilinear Finite-Element Modeling", *IEEE Trans. Antennas and Prop., conditionally accepted with paper revision in progress, 2017*

Conference Papers and Abstracts

[1] M. Ahadi, M. Kabir , et al. "Non-Intrusive Pseudo Spectral Approach for Stochastic Macromodeling of EM Systems using Deterministic Full-wave Solvers", IEEE Conference on Electrical Performance of Electronic Packaging and Systems, 2014

[2] A. Manic, S. Manic, A. Smull, and B. Notaros, "Parallel Double Higher Order Algorithms for Large and Complex Problems Based on Integral and Partial Differential Equations in Computational Sciences Developed for HPC," presented at 2015 RMACC High Performance Computing Symposium, August 12-14, 2015, Boulder, Colorado.

[3] B. M. Notaros, A. B. Manic, A. P. Smull, S. B. Manic, X. S. Li, F-H. Rouet, "Multiscale electromagnetic modeling using double-higher-order quadrilateral meshes and parallel MoM-SIE direct solutions," *2016 IEEE Int. Symp. on Antennas and Propag,* pp. 235-236, IEEE, 2016.

[4] A. P. Smull, A. B. Manic, S. B. Manic and B. M. Notaros, "Double higher-order FEM modeling using an anisotropic conformal perfectly matched layer," *2016 IEEE Int. Symp. on Antennas and Propag,* pp. 1119-1120, IEEE, 2016.